Medial orbitofrontal neurotrophin systems integrate hippocampal input into outcome-specific value representations

Ellen P. Woon[1,2,3], **Laura M. Butkovich**[2,3], **Arianna A. Peluso**[2,3], **Aziz Elbasheir**[1,2,3], **Kian Taylor**[1,2,3], **Shannon L. Gourley**[1,2,3,4,*]

[1]Graduate Training Program in Neuroscience, Emory University, Atlanta, GA 30322, USA

[2]Departments of Pediatrics and Psychiatry, Emory University School of Medicine, Atlanta, GA 30322, USA

[3]Emory National Primate Research Center, Emory University, Atlanta, GA 30322, USA

[4]Lead contact

SUMMARY

In everyday life, we mentally represent possible consequences of our behaviors and integrate specific outcome values into existing knowledge to inform decisions. The medial orbitofrontal cortex (MO) is necessary to adapt behaviors when outcomes are not immediately available—when they and their values need to be envisioned. Nevertheless, neurobiological mechanisms remain unclear. We find that the neuroplasticity-associated neurotrophin receptor tropomyosin receptor kinase B (TrkB) is necessary for mice to integrate outcome-specific value information into choice behavior. This function appears attributable to memory updating (and not retrieval) and the stabilization of dendritic spines on excitatory MO neurons, which led us to investigate inputs to the MO. Ventral hippocampal (vHC)-to-MO projections appear conditionally necessary for value updating, involved in long-term aversion-based value memory updating. Furthermore, vHC-MO-mediated control of choice is TrkB dependent. Altogether, we reveal a vHC-MO connection by which specific value memories are updated, and we position TrkB within this functional circuit.

In brief

Envisioning the possible consequences of our behaviors and integrating their current values into existing knowledge is critical to decision making. Woon et al. identify necessary interactions between the hippocampus and medial orbitofrontal cortex (MO) to update outcome values when they change to guide choice, a process that is dependent on neurotrophin receptor TrkB.

*Correspondence: shannon.l.gourley@emory.edu.

Graphical Abstract
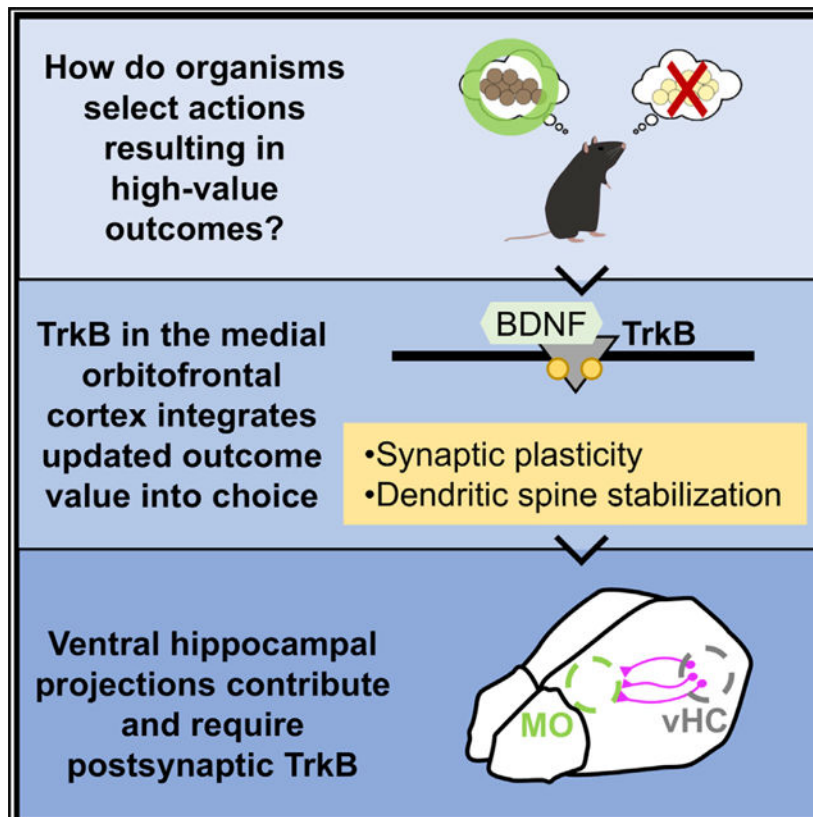
INTRODUCTION

In day-to-day life, we often select our actions based on envisioned outcomes, mentally representing possible consequences of our behaviors and integrating their current values into existing knowledge to inform decisions. For example, one may envision different foods one could eat for lunch (pizza versus hamburger). One incorporates previous experience (Did pizza previously give you food poisoning?) to determine each food's current value to inform choice.

The medial orbitofrontal cortex (MO), positioned at the base of the medial wall of the frontal cortex, is activated when individuals compare different outcome values (Paulus and Frank, 2003) and when the value of an outcome informs action selection (Arana et al., 2003; Plassmann et al., 2007). Furthermore, damage to the MO impairs the ability to "think through" actions, such that patients rely on immediate information to guide their behaviors (Bechara et al., 1994; Schnider et al., 2005, 2013). These findings are consistent with rodent studies demonstrating that the MO facilitates the ability of rodents to adapt their behavior under uncertain circumstances (Dalton et al., 2016; Gourley et al., 2010; Stopper et al., 2012). More recent investigations revealed that the MO is necessary for rodents to make adaptive choices when outcomes are not immediately available and must be envisioned, but not when outcomes are readily available (Bradfield et al., 2015, 2018).

The ability to create mental representations of outcomes and their current values is a crucial component of adaptive decision-making. Here, we investigated how the MO coordinates value-based action from integrated molecular and circuit-level perspectives. We find that the neuroplasticity-associated neurotrophin receptor tropomyosin receptor kinase B (TrkB) is essential for mice to update but not retrieve outcome-specific value information to inform future action selection strategies—a behavior likely attributable, at least in part, to the preservation of intracellular signaling systems supporting the integrity of dendritic spines on excitatory MO neurons.

Dendritic spines are the primary sites of excitatory input on neurons. Thus, we next questioned which inputs could coordinate specific value memory updating. Ventral hippocampus (vHC) inputs to lateral orbitofrontal regions appear to encode features about anticipated outcomes and detect changes in outcome contingencies (Witter, 2006; Barfield and Gourley, 2019; Wikenheiser et al., 2017); however, investigations have to date neglected the MO. We find that vHC connections with the MO modulate value processing under certain circumstances, and this process is TrkB dependent.

RESULTS

TrkB is necessary for value memory updating, but not retrieval

Value-based action refers to engaging behaviors that result in high-value outcomes. Such actions are flexible and modifiable if outcome values change, and require organisms to learn about and update outcome values and then retrieve outcome value memories to guide choice. Brain-derived neurotrophic factor (BDNF) is necessary for value-based action (Gourley et al., 2016), but it remains unclear which phase(s) of learning and memory require BDNF-mediated signaling.

The high-affinity receptor for BDNF is TrkB; thus, we used a TrkB antagonist, ANA-12, to block TrkB during value memory updating versus retrieval (Figure 1A). We first trained naive mice to respond to two food reinforcers. The foods were equally preferred throughout, and response rates are collapsed for simplicity (Figure 1B). Mice were designated to vehicle or ANA-12 conditions, with half receiving injections during subsequent memory-updating periods and half receiving injections during memory-retrieval periods. Importantly, groups did not differ during the initial training period, before any injections (main effect of session $F_{(6,240)} = 46.6, p < 0.001$, no main effect of updating versus retrieval $F < 1$, no main effect of drug $F_{(1,40)} = 0.592$, $p = 0.446$, no interaction session*updating versus retrieval, no interaction session*drug, no interaction session*updating versus retrieval*drug: all $F < 1$).

Next, mice underwent conditioned taste aversion (CTA). Mice were given unlimited access to one type of pellet used during training in a separate, clean cage. Immediately after consumption, mice were injected with LiCl, which induces temporary gastric malaise and reduces the value of the pellet ("devalued"). Meanwhile, the other pellet is paired with saline and retains value ("valued"). Mice assigned to the "value updating" group were administered vehicle or ANA-12 before these sessions. Mice decreased consumption of the devalued pellet, as expected (interaction session* pellet $F_{(4,160)} = 2.40$, $p < 0.001$, main effect of pellet $F_{(1,40)} = 86.53$, $p < 0.001$). Importantly, neither vehicle nor TrkB blockade affected

food consumption during the CTA procedure, relative to each other or the uninjected retrieval groups (no main effect of updating versus retrieval, no main effect of drug, no interaction session* drug, no interaction session*updating versus retrieval, no interaction pellet*updating versus retrieval, no interaction pellet*drug, no interaction pellet*updating versus retrieval *drug, no interaction session*pellet*updating versus retrieval*drug: all $F < 1$) (Figure 1C).

Mice were returned to the conditioning chambers to determine whether they modified their behavior based on the updated value of one pellet (but not the other). Mice assigned to the "memory retrieval" group were injected at this time. Inhibiting TrkB activity during value memory updating, but not retrieval, impaired the ability of mice to engage in value-based action; as such, TrkB blockade during CTA obstructed the ability of mice to later favor the valued pellet (interaction pellet*updating versus retrieval $F_{(1,40)} = 4.232$, $p = 0.046$, interaction pellet*drug $F_{(1,40)} = 4.687$, $p = 0.036$, main effect of pellet $F_{(1,40)} = 16.147$, $p < 0.001$, main effect of drug $F_{(1,40)} = 5.074$, $p = 0.03$, no main effect of updating versus retrieval $F < 1$) (Figure 1D).

Next, we conducted post-probe consumption tests. Mice were given *ad libitum* access to both pellets in a separate, clean cage. All of the groups preferentially consumed the valued pellet (main effect of pellet $F_{(1,40)} = 256.39$, $p < 0.001$). No differences between groups were detected (no main effect of timing $F < 1$, no main effect of drug $F < 1$, no interaction pellet*updating versus retrieval $F_{(1,40)} = 1.875$, $p = 0.178$, no interaction pellet*drug $F < 1$, no interaction pellet*updating versus retrieval*drug $F_{(1,40)} = 1.11$, $p = 0.298$) (Figure 1E). Thus, inhibiting TrkB did not affect CTA, but rather the ability of mice to integrate outcome features into future action strategies. Throughout this report, no manipulation affected food intake during this post-probe test, hereafter reported in Figure S1.

To summarize, TrkB activity is necessary for value memory updating, but not retrieval. As such, blocking TrkB during a memory updating period occludes the ability of mice to adapt future goal-seeking behaviors.

TrkB in the MO is necessary for selective value memory updating

The MO is necessary for flexible goal seeking, particularly when outcomes are unobservable and must be envisioned (Bradfield et al., 2015). We next tested the hypothesis that TrkB in the MO supports this function. We delivered Cre-recombinase (Cre) to the MO of mice that were homozygous for a "floxed" *Ntrk2* gene, which encodes TrkB. A calcium/calmodulin-dependent protein kinase II (CaMKII) promoter restricted knockdown to excitatory neurons, including those that were *Etv1*^{+}, a marker of layer V excitatory neurons (Boyle et al., 2011; Rowell et al., 2010) (layer V forming the primary input/output layer of the cortex) ($t_6 = 3.109$, $p = 0.0209$) (Figures 2A, 2B, and S2). Furthermore, viral vector delivery to the MO resulted in stereotyped terminal patterns in the dorsomedial striatum (Figure 2C), also as expected (Schilman et al., 2008).

Mice were trained to respond to food reinforcers (main effect of session $F_{(6,114)} = 3.343$, $p = 0.004$, no main effect of group, no interaction session*group: all $F < 1$) (Figures 2D and 2E). Next, mice underwent CTA, decreasing consumption of the devalued pellet (interaction

session*pellet $F_{(4,19)}$ = 2.061, p < 0.001, main effect of pellet $F_{(1,19)}$ = 9.228, p < 0.001). Again, no group differences were detected (no main effect of group $F_{(1,19)}$ = 2.444, p = 0.134, no interaction session*group, no interaction session*pellet*group: all F < 1). A pellet*group interaction was detected ($F_{(1,19)}$ = 6.75, p = 0.018), and groups differed on session 4. Importantly, however, no group differences were detected during the final session (Figure 2F).

Mice were returned to the operant conditioning chambers to test whether they adapted behavioral responses based on outcome values. The choice test was conducted under two different conditions: "unobservable" (pellets not delivered, as above) and "observable" (pellets delivered) (Bradfield et al., 2015). When outcomes were unobservable, *Ntrk2* knockdown mice failed to prefer the higher value outcome (interaction pellet*group $F_{(1,19)}$ = 5.021, p = 0.037, main effect of pellet $F_{(1,19)}$ = 8.456, p = 0.009, no main effect of group F < 1) (Figure 2G). Meanwhile, when outcomes were observable, both groups favored the valued pellet (main effect of pellet $F_{(1,19)}$ = 8.421, p = 0.009, no main effect of group F < 1, no interaction pellet*group $F_{(1,19)}$ = 1.573, p = 0.225) (Figure 2H).

In summary, TrkB in the MO appears necessary for mice to engage in value-based action, particularly when outcomes are unobservable and must be inferred. To further solidify this conclusion, we next overexpressed the inactive isoform of TrkB, truncated TrkB (TrkB.t1), in the MO (Figure 2I). TrkB.t1 lacks the intracellular signaling domains necessary for signal propagation. Thus, viral-mediated overexpression of TrkB.t1 interferes with TrkB-mediated signaling, including in the orbitofrontal cortex (Pitts et al., 2018).

Mice were trained to acquire food reinforcers. We detected a main effect of session ($F_{(6,108)}$ = 30.3, p < 0.001) and no effect of TrkB.t1 status (no main effect of group $F_{(1,18)}$ = 1.08, p = 0.313, no interaction of session*group F < 1) (Figure 2J). During CTA, mice decreased consumption of the devalued pellet (interaction session*pellet $F_{(4,72)}$ = 1.42, p = 0.001, main effect of pellet $F_{(1,18)}$ = 50.48, p < 0.001). Again, no group differences were detected (no main effect of group, no interaction session*group, no interaction pellet*group, no interaction session*pellet*group: all F < 1) (Figure 2K).

Mice were returned to the conditioning chambers. When outcomes were unobservable, *Trkb.t1* mice failed to engage in value-based action and responded equivalently for both valued and devalued pellets (interaction pellet*group $F_{(1,18)}$ = 6.58, p = 0.019, no main effect of pellet $F_{(1,18)}$ = 2.33, p = 0.144, no main effect of group F < 1) (Figure 2L). In contrast, when the outcomes were observable (meaning that responses now yielded a food pellet), both groups preferred the valued outcome (main effect of pellet $F_{(1,9)}$ = 5.55, p = 0.043, no main effect of group F < 1, no interaction pellet*group F < 1) (Figure 2M).

In summary, loss of TrkB, via *Ntrk2* knockdown, or TrkB activity, via *Trkb.t1* overexpression, in the MO impairs the ability of mice to favor valued outcomes (as with lesions of the MO; Bradfield et al., 2015). Our experiments using systemic administration of a TrkB antagonist (Figure 1) suggest that TrkB supports the updating of memories regarding outcome-specific values and not memory retrieval. Thus, we next conducted an experiment in which we delayed *Trkb.t1* overexpression in the MO until after the value-updating period

(Figure 2N); if TrkB-mediated signal propagation in the MO is similarly not necessary for memory retrieval, then delayed viral vector delivery should have no effects.

Naive mice were trained to acquire food reinforcers (main effect of session $F_{(6,102)} = 8.258$, $p < 0.001$), with no differences between the mice ultimately given a control versus TrkB.t1 viral vector (no main effect of group, no interaction session*group: all $F < 1$) (Figure 2O). Mice then underwent CTA, decreasing consumption of the devalued pellet (interaction session*pellet $F_{(4,68)} = 12.605$, $p < 0.001$, main effect of pellet $F_{(1,17)} = 13.922$, $p = 0.002$). Again, no group differences were detected (no main effect of group, no interaction session*group, no interaction pellet*group, no interaction session*pellet*group: all $F < 1$) (Figure 2P).

After CTA, mice were infused with viral vectors and then returned to the test chambers. Both groups preferred the valued pellet, regardless of whether outcomes were unobservable (main effect of pellet $F_{(1,17)} = 7.85$, $p = 0.012$, no main effect of group $F_{(1,17)} = 1.245$, $p = 0.28$, no interaction pellet*group $F < 1$) or observable (main effect of pellet $F_{(1,17)} = 8.099$, $p = 0.011$, no main effect of group, no interaction pellet*group: $F < 1$) (Figures 2Q and 2R). Thus, TrkB activity in the MO is necessary for selective value memory updating, but not retrieval.

TrkB-mediated signaling controls dendritic spine density and structure on excitatory MO neurons

TrkB coordinates a number of neurobiological processes, including dendritic spine stability, a likely controller of behavior, given that dendritic spines form the principal sites of excitatory inputs in the brain. We imaged layer V MO neurons expressing *Trkb.t1* or a control viral vector (Figures 3A and 3B), revealing that *Trkb.t1* overexpression reduced mature, mushroom-shaped spine densities ($t_{(10)} = 2.70$, $p = 0.022$). Meanwhile, immature stubby- and thin-type spines were unaffected ($t_{(10)} = 1.94$, $p = 0.081$; $t_{(10)} = 0.969$, $p = 0.355$) (Figure 3C). Mushroom-shaped spines were also longer in the *Trkb.t1* overexpression group ($t_{(422)} = -1.745$, $p = 0.041$) (Figures 3D and S3). When all of the dendritic spines were measured, *Trkb.t1*-overexpressing spines were again longer as a population ($D = 0.104$, $p = 0.003$) (Figure 3E), an effect localized to shorter spines (lower 50th percentile $D = 0.1881$, $p < 0.001$; upper 50th percentile $D = 0.0898$, $p = 0.1861$). This pattern may reflect the inability of *Trkb.t1*-overexpressing spines to appropriately retract from a long, immature shape to a shorter, mature (mushroom) shape. This phenomenon would account for overall lower densities of mature spines in the *Trkb.t1* group (again, Figure 3C). No effects on spine clustering—referring to tightly grouped spine assemblies—were detected (Figure S3).

TrkB controls dendritic spine plasticity in part via the phosphatidylinositol 3-kinase (PI3K) signaling complex, composed of p110 catalytic and p85 regulatory subunits. The p110δ subunit is associated with receptor tyrosine kinases and regulates dendritic spine structure via the RhoA GTPase (Figure 4A). We thus generated a small hairpin RNA (shRNA) against *Pik3cd*, which encodes p110δ, restricting expression to excitatory neurons. If dendritic spine structure and plasticity are causally related to the control of action selection by TrkB, then we reasoned that silencing *Pik3cd* in the MO (Figure 4B) should recapitulate the behavioral effects of inhibiting TrkB.

Mice were trained to respond to food reinforcers (main effect of session $F_{(6,54)} = 4.228$, p = 0.001), and no group differences were detected (no main effect of group, no interaction of session*group: F < 1) (Figure 4C). Mice next underwent CTA, decreasing the consumption of the devalued pellet (interaction session*pellet $F_{(4,36)} = 23.006$, p < 0.001, main effect of pellet $F_{(1,9)} = 40.083$, p < 0.001). Again, no group differences were detected (no main effect of group F < 1, no interaction session*group $F_{(4,36)} = 1.188$, p = 1.188, no interaction of pellet* group, no interaction of session*pellet*group: F < 1) (Figure 4D).

Mice were then returned to the conditioning chambers. Reduction of p110δ in the MO impaired value-based action (interaction pellet type*group $F_{(1,9)} = 14.402$, p = 0.004; no main effect of pellet, no main effect of group: F < 1) (Figure 4E). *Pik3cd* knockdown mice even appeared to favor the devalued pellet, but further analyses revealed that response rates were simply unchanged from the last training session before CTA (Figure S4A). Thus, silencing the TrkB-associated PI3K p110δ occludes the ability of mice to select actions based on outcomes.

vHC-to-MO projections are necessary for mice to use value information to guide future choice under specific circumstances

Our findings suggest that TrkB supports value-based action at least in part via the stabilization of dendritic spines, the primary sites of excitatory inputs onto neurons. This observation leads to the question: What inputs to the MO provide information to guide action? The vHC sends monosynaptic projections to the MO (Jay and Witter, 1991; Witter, 2006), a well-documented pattern in rats that we duplicated here via fluoro-ruby tracing in mice (Figure 5A). We next delivered a retrograde Cre-expressing viral vector into the MO, and Cre-dependent (DIO) Gi-coupled designer receptor exclusively activated by designer drugs (Gi-DREADDs) into the vHC (Figure 5A). This combination of viral vectors allows for the inactivation of vHC-to-MO projections, evidenced by decreased immediate-early gene c-Fos expression in the Gi-DREADDs versus Cre-dependent mCherry condition ($t_{(8)} = 4.888$, p = 0.001) (Figure 5B).

Mice were trained to respond to food reinforcers in the absence of the DREADD ligand clozapine *N*-oxide (CNO). We detected a main effect of session ($F_{(6,246)} = 55.082$, p < 0.001) and session*group interaction ($F_{(6,246)} = 2.907$, p = 0.009). Post hoc analyses revealed that groups differed on sessions 5–6, likely a spurious consequence of modest cohort differences. No group differences were detected on the final session (Figure 5C). We also detected no main effect of group ($F_{(1,41)} = 1.867$, p = 0.179).

Next, mice underwent CTA, and all of the mice, regardless of viral vector group, were administered CNO before each session. Thus, vHC-to-MO projections were inactivated in mice expressing Gi-DREADDs during this value-updating period. Mice decreased their consumption of the devalued pellet (interaction session*pellet $F_{(4,164)} = 80.847$, p < 0.001, main effect of pellet $F_{(1,41)} = 61.002$, p < 0.001). No group differences were detected (no main effect of group F < 1, no interaction session*group $F_{(4,164)} = 1.817$, p = 0.128, no interaction pellet*group, no interaction session*pellet*group: all F < 1) (Figure 5D).

Then, mice were returned to the conditioning chambers. Inactivation of vHC-to-MO projections during value updating impaired the ability of mice to use outcome-specific information to influence choice, such that inactivation mice responded equivalently for devalued and valued outcomes (interaction pellet*group $F_{(1,41)} = 5.028$, $p = 0.03$, main effect of pellet $F_{(1,41)} = 7.184$, $p = 0.011$, no main effect of group $F < 1$) (Figure 5E). Thus, vHC-to-MO projections appear necessary to update outcome value information for future choice. The vHC also innervates the adjacent, ventrolateral orbitofrontal cortex, but notably, we found no effects if we chemogenetically inactivated neurons in this region using identical procedures (Figure S5), supporting the notion that these subregions are functionally distinct, and that the ventrolateral region may be particularly attuned to reward contingency or scenarios in which value and contingency information must be integrated (Parkes et al., 2017; Li et al., 2022).

What information might the vHC convey? Considering the role of the vHC in emotion processing (Fanselow and Dong, 2010), we hypothesized that the emotive content associated with CTA (i.e., fear of bodily harm due to toxin) recruits the vHC. This possibility led to the prediction that a devaluation procedure that does not produce a strong emotive response would not involve vHC processing. Thus, we turned to satiety-specific prefeeding; in this case, mice received *ad libitum* access to one of the pellets before the choice test, thus devaluing that pellet. Decreased responding during the choice test reflects value-based choice (Figure 5F). As a control for satiety, mice were given *ad libitum* access to vivarium chow before a separate choice test. In this case, mice still became sated, but the pellets were not devalued.

Again, mice were administered CNO before the prefeeding period, when value memory was being updated. Food consumption did not differ between groups (all $F < 1$). During the choice test, both groups inhibited responding for the devalued pellet, able to use value to guide actions (main effect of pellet $F_{(1,22)} = 35.848$, $p < 0.001$, no main effect of group, no food*group interaction: all $F < 1$) (Figure 5G). Thus, vHC-to-MO connections may process emotive information, rather than playing a generalized role in value processing.

vHC-MO coordination of value-based action requires TrkB

We hypothesized that vHC-to-MO projections contribute to value-based action in a TrkB-dependent manner. We capitalized on the unidirectional, ipsilateral nature of vHC-to-MO connections—in other words, the left vHC innervates the left MO and the right innervates the right, with minimal crossing fibers (Laroche et al., 2000). We overexpressed *Trkb.t1* in one hemisphere of the MO and infused Gi-DREADDs into the contralateral vHC (Figures 6A and 6B). Thus, with the administration of CNO, an inactivated vHC projects to a healthy MO in one hemisphere. In the other hemisphere, a healthy vHC projects to a TrkB activity-deficient MO. If value-based action involves TrkB-dependent vHC-MO interactions, then mice will fail to exhibit value-based action. In the control group, *Trkb.t1* was unilaterally overexpressed in the MO and Gi-DREADDs placed in the ipsilateral vHC. This design leaves one hemisphere intact.

We again confirmed that Gi-DREADDs decreased c-Fos as expected (DREADD versus control hemisphere, paired $t_{(5)} = 3.382$, $p = 0.02$) (Figure 6C). Mice were trained to respond

to food reinforcers (main effect of session $F_{(6,132)} = 9.91$, $p < 0.001$). No group differences were detected (no main effect of group, no interaction session*group: all $F < 1$) (Figure 6D). Then, mice underwent CTA, and CNO was administered. Mice decreased consumption of the devalued food (interaction session*pellet $F_{(4,88)} = 47.693$, $p < 0.001$, main effect of pellet $F_{(1,22)} = 311.395$, $p < 0.001$). No group differences were detected (no main effect of group $F < 1$, no interaction session*group $F_{(4,88)} = 1.913$, $p = 0.115$, no interaction pellet*group $F < 1$, no interaction session*pellet*group $F_{(4,88)} = 1.57$, $p = 0.189$) (Figure 6E).

Finally, mice underwent a choice test drug-free. Contralateral infusions impaired the ability of the mice to use outcome information to influence action, responding similarly for the valued versus devalued pellets (interaction pellet*group $F_{(1,22)} = 15.17$, $p < 0.001$, no main effect of pellet $F < 1$, no main effect of group $F_{(1,22)} = 2.013$, $p = 0.17$) (Figure 6F). Further solidifying this point, contralateral mice responded equivalently for a food before versus after it was devalued (Figure S4B). Thus, value-based action selection following CTA requires TrkB-dependent vHC-MO interactions.

We next tested mice using a prefeeding devaluation procedure, as above. Both groups inhibited responding when prefed pellets (main effect of pellet $F_{(1,20)} = 16.409$, $p < 0.001$, main effect of group $F_{(1,20)} = 6.055$, $p = 0.023$, no interaction pellet*group $F_{(1,20)} = 4.143$, $p = 0.055$), indicating that vHC-MO connections are dispensable for value-based actions following prefeeding (Figure 6G).

In summary, outcome-specific value updating appears to recruit vHC-to-MO connections under particular circumstances, implying that disrupting vHC function should disrupt the same processes. To test this prediction, Gi-DREADDs were bilaterally infused into the vHC (Figure 7A). Mice were trained to respond to food reinforcers (main effect of session $F_{(6,120)} = 18.647$, $p < 0.001$), with no group differences (no main effect of group, no interaction session*group: all $F < 1$) (Figure 7B). Then, mice underwent CTA, and CNO was administered. Mice decreased consumption of the devalued pellet (interaction session*pellet $F_{(4,80)} = 30.083$, $p < 0.001$, main effect of pellet $F_{(1,20)} = 36.627$, $p < 0.001$), and no group differences were detected (no main effect of group $F_{(1,20)} = 1.70$, $p = 0.207$, no session*group interaction pellet $F_{(4,80)} = 1.231$, $p = 0.304$, no pellet*group interaction, no session*pellet*group interaction: $F < 1$) (Figure 7C).

Finally, mice underwent the choice test drug-free. Chemogenetic inhibition of the vHC during the value updating period impaired value-based action, as anticipated (interaction pellet* group $F_{(1,20)} = 4.267$, $p = 0.05$, main effect of pellet $F_{(1,20)} = 9.414$, $p = 0.006$, no main effect of group $F < 1$) (Figure 7D).

Synaptic connections on excitatory neurons in the hippocampus require a cell adhesion receptor called β1-integrin (Warren et al., 2012). As a final experiment, we used mice that were homozygous for a floxed *Itgb1* gene, which encodes β1-integrin, and infused adeno-associated virus (AAV)-CaMKII ± Cre to reduce β1-integrin protein. Mice were then trained to respond for food reinforcers (main effect of session $F_{(6,126)} = 5.915$, $p < 0.001$), with no group differences (no main effect of group $F < 1$, no interaction session*group

$F_{(6,126)} = 1.015$, $p = 0.419$) (Figure 7E). During CTA, mice decreased consumption of the devalued pellet (interaction session*pellet $F_{(4,84)} = 15.646$, $p < 0.001$, main effect of pellet $F_{(1,21)} = 20.461$, $p < 0.001$). No group differences were detected (no main effect of group $F < 1$, no interaction session*group $F_{(4,84)} = 1.474$, $p = 0.217$, no interaction pellet*group $F < 1$, no interaction session*pellet*group $F_{(4,84)} = 1.411$, $p = 0.237$) (Figure 7F).

Finally, mice were returned to the conditioning chambers. As predicted, loss of β1-integrin in the vHC impaired value-based action (interaction pellet*group $F_{(1,22)} = 4.199$, $p = 0.05$, main effect of pellet $F_{(1,22)} = 16.177$, $p < 0.001$, no main effect of group $F_{(1,22)} = 2.247$, $p = 0.148$), further indicating that the vHC is essential for value-based choice following CTA (Figure 7G).

DISCUSSION

Research on the orbitofrontal cortex has exploded recently, driven in part by perceived homologies between rodents and primates (Izquierdo, 2017; Rudebeck and Izquierdo, 2022; Wallis, 2011). Nevertheless, most of the investigations in rodents focus on lateral subregions, largely neglecting the MO. Bradfield et al. (2015) reported that pre-training lesions or chemogenetic inhibition of the MO impairs the ability of rats to select actions based on likely outcomes. We find that TrkB-mediated signaling in the MO is similarly necessary for value-based decision making, such that blocking neuronal TrkB when a food loses value impedes the ability of mice to integrate new value into future action, even while aversion to the food is intact. What was unexpected, however, was that TrkB was consistently involved in value memory updating, while prior investigations had largely implicated the MO in memory retrieval (Bradfield and Hart, 2020). This insight led to our discovery that vHC-to-MO interactions are necessary for outcome-specific value memory updating under certain circumstances, requiring TrkB.

TrkB is necessary for value-based action

Here, we trained mice to respond to two distinct food outcomes. We then decreased the value of one outcome using CTA, in which mice freely consume one food, then are injected with LiCl, producing gastric malaise and devaluing that outcome. Meanwhile, the other outcome remains valued. Later, mice are returned to the conditioning chambers for a brief choice test. Thus, value updating for specific outcomes, occurring during CTA, is dissociable from memory retrieval—when mice make choices. Inhibiting TrkB activity during value memory updating but not retrieval impaired the ability of mice to use value information to guide choice. Thus, TrkB activity is necessary to update outcome value.

Next, we reduced *Ntrk2*, or overexpressed the dominant negative isoform of TrkB, TrkB.t1, in the MO. Loss of TrkB or its activity occluded value-based action, this effect again attributable to disrupted memory, since overexpressing *Trkb.t1* later, after memory updating, had no effects. Notably, action selection was disrupted only when outcomes were not delivered and thus needed to be envisioned. When outcomes were observable, value-based action was intact, supporting the notion that the MO represents abstract outcomes, rather than integrating sensory information into ongoing action (Bradfield and Hart, 2020; Kringelbach and Rolls, 2004).

In the MO, neuronal firing is associated with the ability to predict outcomes of low value (Burton et al., 2014). Given that *Trkb.t1* overexpression imperils synaptic plasticity (Michaelsen et al., 2010), one could imagine that *Trkb.t1* overexpression in the MO causes mice to resist behavioral shifts following outcome devaluation because impoverished outcome values are unable to be integrated into action. If outcome values become muddied, then this could even discourage any responding at all (Balleine, 2020), which would account for generally low response rates in rats with MO lesions (Bradfield et al., 2015) and some mice here, most notably with *Trkb.t1* overexpression. This *Trkb.t1* experiment used a lentiviral vector, which transduces neurons and some glial subtypes (Ehrengruber et al., 2001) (while other experiments used more selective strategies), so it may be sensible that these mice most closely resemble organisms with gross lesions.

Identifying substrates and connections for prospective action selection

Dendritic spines house the majority of excitatory synapses in the brain and rely upon TrkB-mediated signaling for stabilization (Barfield and Gourley, 2018) throughout cortical layers (Galloway et al., 2008; Hayashi et al., 2000). Here, we visualized layer V neurons, because they are sites of input from subcortical structures, and also form the primary output layer and source of BDNF in the cortex (Hartmann et al., 2001). *Trkb.t1* overexpression decreased the density of mushroom-shaped spines, which contain the largest excitatory synapses, necessary for long-term potentiation (LTP) (Berry and Nedivi, 2017). It also lengthened the remaining spines, consistent with reports concerning the primary visual cortex (Chakravarthy et al., 2006) and hippocampus (Hartmann et al., 2004), and significant because long spine necks can fail to generate somatic depolarizations (Araya et al., 2014).

One pathway by which TrkB binding controls actin cytoskeleton rearrangements engages the PI3K signaling complex, composed of p110 catalytic and p85 regulatory subunits. p110δ is associated with receptor tyrosine kinases and inhibits the small guanosine triphosphatase (GTPase) RhoA (Eickholt et al., 2007; Papakonstanti et al., 2007), which regulates spine structure through Rho kinase and cofilin. Reducing PI3K p110δ would increase Rho kinase activity, potentially preventing dendritic spine plasticity, including morphological stabilization, a process that requires the retraction of thin-type spines into mature, mushroom shapes (dos Remedios et al., 2003; Pontrello and Ethell, 2009). We reasoned that if TrkB-mediated dendritic spine stabilization facilitates value-based action, then silencing TrkB signaling partners that link TrkB with actin cytoskeleton regulation should have the same effects as TrkB inhibition. As anticipated, reducing p110δ in the MO occluded value-based choice.

Altogether, then, evidence points to postsynaptic MO neurons as substrates for specific value memory, leading to the question: What signals are they receiving? The MO receives input from the basolateral amygdalar (BLA) (Hoover and Vertes, 2011), but these projections are not necessary for outcome value updating (Lichtenberg et al., 2021). Another candidate is the vHC, which is necessary for lateral orbitofrontal cortical neurons to encode features about anticipated outcomes (Wikenheiser et al., 2017), and lesions of the MO and vHC have identical consequences in an instrumental reversal task (Gourley et al., 2010). Here, we inactivated vHC-to-MO projections during value memory updating, then tested choice

behavior, drug-free. Mice were unable to select actions resulting in high-value rewards, indicating that vHC-to-MO connections are necessary for value memory following CTA.

The vHC controls emotion processing (Bryant and Barker, 2020; Fanselow and Dong, 2010). We hypothesized that vHC connections convey emotive content associated with CTA (i.e., fear of bodily harm due to toxin) to the MO for integration into outcome representation, leading to the prediction that if outcome values changed in a way that was presumably less emotive, vHC connections would be dispensable for action flexibility. To test this possibility, we devalued food using satiety, and indeed, all of the mice favored the valued outcome in this situation. We also confirmed that CTA caused conditioned object aversion, while satiety did not, evidence that satiety is not aversive (Figure S6). Thus, the vHC appears to integrate outcome-specific value information into choice behavior, but only under certain circumstances. Further supporting this notion, chemogenetically silencing excitatory neurons in the vHC, or silencing *Itgb1*, which encodes the β1-integrin cell adhesion protein that anchors excitatory neurons in the hippocampus (Warren et al., 2012), disrupted memory updating triggered by CTA.

We next investigated whether functional vHC-to-MO connections require TrkB. vHC-to-MO projections are overwhelmingly ipsilateral (Laroche et al., 2000), allowing us to use a "disconnection" experimental design. We placed *Trkb.t1* in one hemisphere of the MO and inhibitory Gi-DREADDs into the ipsilateral or contralateral vHC. Upon administration of a DREADDs ligand, mice with contralateral infusions have an inactivated vHC projecting to a healthy MO in one hemisphere and a healthy vHC interacting with a *Trkb.t1*-expressing MO. If value processing requires TrkB-dependent vHC-MO interactions, then mice will fail to update specific value memories, which was indeed the case. Meanwhile, control mice received ipsilateral infusions, leaving one hemisphere intact, which was sufficient for value memory updating upon CTA.

Conclusions

MO function has become clearer in recent years, owing to experiments using inducible and projection-specific manipulations (Jenni et al., 2022; Lichtenberg et al., 2021; Loh et al., 2022; Malvaez et al., 2019). Other investigators have unveiled local neurotransmitter systems necessary for motivated responding (Jenni et al., 2021; Münster et al., 2020). Less clear are which neuromodulators act within defined circuits. Our findings reveal a vHC-MO connection that modulates value-based choice, and we position TrkB and one of its substrates, PI3K p110δ, as well as the cell adhesion protein β1-integrin, within this functional circuit. *ITGB1* is identified in genome-wide association studies of schizophrenia (Chang et al., 2015), and TrkB-PI3K signaling has long been implicated in depression etiology (Matsuda et al., 2019; Wang et al., 2022). Our findings may thus shed light onto mechanistic factors controlling decision-making behavior in healthy individuals, and its disruption in neuropsychiatric illness, in which aberrant decision-making can be symptomatic, and even reinforcing, of illness (Nakao et al., 2014; Rudebeck and Rich, 2018).

Limitations of the study

Collectively, these findings reveal that the vHC modulates MO function, with the vHC potentially supplying emotive information in a TrkB-dependent manner. An alternative interpretation is that the vHC instead transmits current state information to the MO. State dependence refers to the phenomenon by which organisms recall information better if they are in the same physical or mental state as when they learned it. If the vHC transmits state information, then mice with inactivated vHC-to-MO connections during CTA may be impaired later at the choice test due to the inability to access state information. By the same token, responding following prefeeding would be unaffected because mice are in the same "state" during both phases as they occur in close temporal proximity. We question this possibility, however, because vHC-selective *Itgb1* knockdown induced gene loss in both memory updating and retrieval periods in a CTA-based devaluation test. As such, mice were in the same state during both testing phases and yet still failed to adapt action strategies. Thus, a state dependence explanation is not obviously supported. Another possibility is that the vHC modulates long-term memory encoding and associated neurosequelae such as dendrite remodeling, while more rapid value processing requiring working memory involves other structures. This possibility would explain why vHC silencing obstructed response plasticity in CTA-but not satiety-based devaluation, and could be tested in future investigations.

Another consideration in our projection-specific inactivation experiments is that vHC projections to the MO can collateralize to the insular cortex (IC) (Verwer et al., 1997). We think that these collaterals likely did not grossly affect outcomes here, because the IC is associated with Pavlovian (and not instrumental) conditioning (Kusumoto-Yoshida et al., 2015; Nasser et al., 2018; Parkes et al., 2016), including CTA (Ferreira et al., 2002; Gutiérrez et al., 1999), such that inactivation disrupts avoidance of a LiCl-paired food. By contrast, none of our manipulations disrupted CTA, and we did not detect fluorescence in the IC in projection-specific inactivation experiments, suggesting that IC collaterals were sparse and did not grossly affect our experiments (Figure S6).

A recent study by Jenni and colleagues (Jenni et al., 2022) reported that MO-to-nucleus accumbens projections are necessary to establish and crystalize choice strategy during tasks that assess risky decision-making. Meanwhile, MO-to-dorsomedial striatum projections are necessary for shifting strategies, such that inactivation caused rats to persist in familiar response sequences even when not profitable, reminiscent of response patterns reported here. These investigations highlight how multiple MO neurocircuits likely operate in tandem to translate value processing into flexible action, an important topic for continued investigation.

STAR★METHODS

RESOURCE AVAILABILITY

Lead contact—Further information and requests for resources and reagents should be directed to the lead contact, Shannon Gourley (shannon.l.gourley@emory.edu).

Materials availability—This study did not generate new unique reagents.

Data and code availability

- The published article includes all data generated and analyzed during this study. Raw data are available from the lead contact upon reasonable request.

- No new code was generated.

- Any additional information required to reanalyze the data reported in this paper is available from the lead contact upon request

EXPERIMENTAL MODEL AND SUBJECT DETAILS

Several strains of mice were used and, unless otherwise noted, bred in-house from Jackson Laboratories stock for use in this study—Subjects were adult postnatal day (P) 56 + C57BL/6 mice (stock #000664). Or, mice were homozygous for either a "floxed" *Ntrk2* gene (He et al., 2004) (sourced from Dr. Keqiang Ye at Emory University, USA), or an *Itgb1* gene (Raghavan et al., 2000) (stock #004605). In experiments examining dendritic spines, imaging was accomplished using *Thy1*-Yellow Fluorescent Protein (YFP)-expressing mice (Feng et al., 2000) (H line, stock #003782) back-crossed onto a C57BL/6 background.

Initial experiments were conducted using male mice. As the project evolved, the inclusion of both sexes became a priority. As such, the final figures in this manuscript (Figures 4, 5, 6, and 7) included both sexes. One sex effect was identified, and statistical approaches are discussed in the quantification and statistical analysis section.

Mice were maintained on a 14-h light cycle (0700 on). Mice were provided food and water *ad libitum* except during instrumental conditioning when body weights were reduced to 90% of baseline to motivate responding. All procedures were approved by Emory University IACUC.

METHOD DETAILS

Intracranial surgery—Mice were anesthetized with 100 mg/kg ketamine/0.5 mg/kg dexdormitor *i.p.* and placed in a digitized stereotaxic frame (Stoelting). The scalp was incised, the head leveled, and needles were centered at Bregma on a leveled skull. Infusions targeted the MO (coordinates: AP+2.8, ML±0.15, DV-2.3; 0.5μL/site over 5 min), vHC (coordinates: AP-2.5, ML±3.6, DV-4.5 and AP-2.7, ML ± −3.2, DV-5.0; 0.25μL/site over 5 min; flruoruby 0.04μL infusion over the course of 3 min), or ventrolateral orbitofrontal cortex (coordinates: AP+2.6, ML±1.2, DV-2.8; 0.5μL/site over 5 min). Needles were left in place for an additional 5 min following infusion, withdrawn, and scalp sutured. Mice were administered 2 mg/kg antisedan *i.p.* For pain management, mice were administered 5 mg/kg meloxicam *s.c.* for 2 days. Mice were left undisturbed for 3 weeks to allow for recovery and viral vector expression.

Ntrk2 knockdown—AAV2/5-CaMKII-mCherry ± Cre (University of North Carolina Viral Vector Core) was delivered bilaterally into the MO of *Ntrk2*-flox mice.

Trkb.t1 overexpression—Lentiviral vectors expressing Green Fluorescent Protein (LV-CMV-GFP) or *Trkb.t1* (LV-CMV-Trkb.t1) tagged with HA (Emory University Viral Vector Core) was delivered into the MO. This viral vector interferes with TrkB-mediated signaling, *in vivo*, including in the orbitofrontal cortex (Pitts et al., 2018). In experiments examining dendritic spines, the control viral vector expressed Red Fluorescent Protein (Emory University Viral Vector Core).

Pik3cd knockdown—AAV2-CaMKII-mCherry ± sh-*Pik3cd* (Vector Biolabs) was delivered bilaterally into the MO. This viral vector was validated by Vector Biolabs, confirming 70% knockdown in screening.

Fluoro-ruby—Fluoro-ruby (Millipore; 10% solution in distilled water) was bilaterally infused into the vHC.

Projection-specific manipulations—Retrograde AAV (AAVrg)-hSyn-HI-eGFP-Cre-GFP-WPRE-SV40 (Addgene) was delivered bilaterally into the MO. AAV5-hSyn-DIO-mCherry ± hM4D(Gi) (Addgene) was delivered bilaterally in the vHC.

Chemogenetic inhibition—AAV5-CaMKII-mCherry ± hM4D(Gi) (Addgene) were delivered into the vHC or ventrolateral orbitofrontal cortex.

Itgb1 knockdown—*Itgb1*-flox mice received bilateral infusions of AAV2/5-CaMKII-mCherry ± Cre (University of North Carolina Viral Vector Core) into the vHC. This procedure reduces local β1-integrin protein content by ~20–40% when gross tissue punches are separated by western blot (DePoy et al., 2019; Kietzman et al., 2022). Note that incomplete protein loss is expected, given that tissue punches processed by western blot contain both transduced and unaffected tissues, and CaMKII-driven AAVs spare glial β1-integrins, which are expressed at high levels (Cahoy et al., 2008).

Instrumental response training—Mice were trained to nose poke for 2 distinct food reinforcers (20 mg purified grain- or chocolate-based pellets; Bioserv) using illuminated Med-Associates conditioning chambers equipped with 2 nose poke recesses and a food delivery magazine. Importantly, these flavors were chosen because mice do not systematically prefer one over another. Mice were trained on a fixed ratio 1 (FR1) schedule of reinforcement, with 30 pellets available for responding on each nose poke aperture, resulting in 60 pellets/session. Sessions concluded at 70 min or when mice acquired all 60 pellets. To acquire all 60 pellets within the allotted time, mice required 7–16 training sessions, and the final 7 sessions are shown.

Conditioned taste aversion (CTA)—Mice were placed in clean chambers with *ad libitum* access to 1 of 2 food pellets used during training. Male mice were allowed to feed for 30 min and females for 60 min. (Females require longer to consume the pellets, hence the longer prefeeding period.) Immediately following, mice were injected with 0.15M lithium chloride (LiCl) in saline (4mL/100g, *i.p.*; Sharp et al., 2017), which induces temporary gastric malaise and conditioned aversion to the now "devalued" pellet. The following day, mice were given access to the other type of pellet used during training,

allowed to feed, and then immediately injected with saline (4mL/100g, *i.p.*). This injection induces no gastric malaise. Thus, this pellet is the "valued" pellet. This procedure was conducted for at least 10 days (5 LiCl and 5 saline pairings). Mice underwent 2 additional pairings (2 LiCl and 2 saline) if they did not reduce intake of the LiCl-paired food within the first 10 days. The pellet paired with LiCl was the one that mice had acquired most during training.

Choice test—Mice underwent a brief choice test in the operant conditioning chambers to determine whether they were able to modify their behavior based on the values of the pellets. Throughout, the choice test was conducted in extinction, *i.e.*, the pellets were not delivered ("unobservable" condition). In some cases, a reinforced choice test was conducted the following day ("observable" condition).

Post-probe consumption test—Following the choice tests, we conducted post-probe consumption tests, in which case, mice were placed in clean chambers with *ad libitum* access to both pellets. Male mice were allowed to feed for 30 min, while females were allowed to feed for 60 min. The amount of food consumed was then measured.

Satiety-specific devaluation—Trained mice were allowed *ad libitum* access to one of the pellets used during training in clean chambers for 60 min. Immediately following, mice were placed in operant conditioning chambers for a brief choice test conducted in extinction. The next day, mice were given *ad libitum* access to their regular chow (LabDiet, 5001), allowed to feed, and underwent another brief choice test in extinction (as in Parkes et al., 2017). Pre-feeding sessions (pellet *vs.* chow) were counterbalanced.

Conditioned object aversion—To confirm that CTA was aversive, as we presume, we conducted an object aversion test. In this case, we paired one object with the CTA procedure and for comparison, another object with the satiety-specific prefeeding devaluation procedure, which is presumably not aversive. Mice were allowed to consume one of the pellets (for instance, chocolate) used during training in clean chambers (30 min for males, 60 min for females). Mice were then immediately injected with LiCl and placed back in the chamber with an object (for instance, a conical tube) for 1 h. Thus, the gastric malaise induced by LiCl was associated with both the chocolate pellet and the conical tube. The next day, mice were allowed to consume the grain pellet, injected with saline, and placed back in the chambers with another object, in this case, a rodent enrichment toy. Here, the satiety sensation was associated with both the grain pellet and the toy. This procedure was conducted for at least 14 days (7 LiCl and 7 saline pairings). When all pairings were completed, the conical tube and toy were secured to the floor of opposite ends of chambers equipped with infrared beams to monitor locomotor activity and quantify proximity to the objects. If LiCl produces an aversive response, mice should avoid the conical tube. If LiCl and satiety produce comparable responses, then mice should not exhibit a preference. Importantly, to habituate mice to the locomotor chambers, mice were placed in the chambers without the objects on the day prior to test.

Drugs (preparation and administration)—In experiments using the TrkB antagonist, ANA-12, mice were administered (*i.p.*) ANA-12 (Millipore Sigma; 0.5 mg/kg, 1mL/100g, as

in Barfield and Gourley, 2017) dissolved in 1% DMSO, or vehicle. ANA-12 or vehicle was administered 3 h (Cazorla et al., 2011) prior to CTA sessions – when outcome value is being updated – or before the choice test – when mice must retrieve memories about the value of outcomes to guide their actions.

In experiments using DREADDs, CNO (Sigma; 1 mg/kg, 1mL/100g) was dissolved in 2% DMSO and saline. CNO was administered immediately prior to CTA sessions. CNO can be back metabolized to clozapine (Gomez et al., 2017; Manvich et al., 2018), but at this dose, there is no detectable plasma clozapine or N-desmethylclozapine (Manvich et al., 2018). In the orbitofrontal cortex, phosphorylated ERK1/2, commonly used as a marker of synaptic plasticity, is unaffected at this dose (Whyte et al., 2019). Nevertheless, all mice received CNO regardless of viral vector group in order to control for any unanticipated consequences of the drug. The choice test occurred 24 h after the last CTA session, when the drug was no longer on board.

Histological procedures and immunostaining—Mice were deeply anesthetized and transcardially perfused with 4% paraformaldehyde. Brains were extracted and placed in chilled 4% paraformaldehyde for 24 h, and then stored in 30% w/v sucrose prior to sectioning at 50mm. Sections were mounted and coverslipped with Vectashield Mounting Medium ± DAPI. Infusion sites were verified by imaging for GFP or mCherry. Mice with mis-targeted infusion sites were excluded from analyses (Table S1).

HA tag immunostaining—To identify infusion sites for the *Trkb.t1* virus, we stained for the HA tag. Sections were blocked in a solution containing 2% normal goat serum (NGS), 1% bovine serum albumin (BSA), and 0.03% Triton X-100 (Sigma) for 1 h at room temperature. Then, sections were incubated with a primary antibody solution containing anti-HA (1:250; Millipore Sigma), 2% NGS, 1% BSA, and 0.03% Triton X-100 at room temperature overnight. Sections were then incubated in a solution containing biotinylated secondary antibody (1:1000; Vector Laboratories), 1% NGS, and 0.03% Triton X-100 at room temperature for 1 h. HA signal was amplified by incubating sections in streptavidin Cy5 or Dylight 594 (15μ/mL; Vector Laboratories) for 30 min. Sections were mounted and coverslipped.

c-Fos immunostaining—To stimulate neuronal activity and thereby generate the resolution to verify *decreased* activity in mice bearing Gi-DREADDs, mice were exposed to the forced swim test. A glass cylinder (24 cm × 15.5 cm diameter) was filled with 25°C water. CNO was administered 30 min prior to testing. After 6 min, mice were dried and placed in a warm cage. After 60 min, brains were collected.

Sections were blocked in a solution containing 2% NGS, 1% BSA, and 0.03% Triton X-100 (Sigma) for 90 min at room temperature. Then, sections were incubated with the primary antibody solution containing anti-c-Fos (1:500; Abcam), 2% NGS, and 0.03% Triton X-100 at 4°C overnight. Sections were then incubated in a secondary antibody solution containing Alexa Fluor 488 or 647 (1:500; Life Technologies), 2% NGS, and 0.03% Triton X-100 at room temperature for 1 h. Sections were mounted and coverslipped.

c-Fos quantification—Immunostained sections were imaged using a Keyence BZ-X710 microscope. vHC images were obtained at 10× magnification. MO images were obtained at 20× magnification. For each experiment, uniform exposure parameters were used throughout, and anatomical landmarks were used to ensure that images were similarly localized.

For c-Fos quantification, analyses were performed using ImageJ software. The analysis pipeline included drawing a standardized region of interest (ROI), background subtracting, intensity thresholding (Otsu method), and automated cell counting within the defined ROI (as in Lustberg et al., 2020). For each experiment, the ROI remained uniform throughout.

Fluoro-ruby imaging—Fluoro-ruby positive axon terminal puncta in the MO were imaged using a spinning disk confocal microscope (VisiTech International) on a Leica microscope. Z-stacks were collected using a 0.2μm step size with a 100×1.4NA objective lens and were then collapsed into a maximum intensity projection using ImageJ software.

Ntrk2 quantification—Mice were euthanized and brains stored in PFA as previously described. Brains were then incubated overnight in sucrose solutions increasing in concentration (10%, 20%, 30%) over 3 days, then flash frozen and stored at −80°C. Sections were collected at 12μm on a CryoStar NX70 cryostat and stored at −80°C on Superfrost Plus Slides. To prevent tissue detachment, steps described in the ACD Technical Note (ACD #320535-TN) were included immediately prior to RNA analysis. *In situ* RNA analysis was completed with the RNAScope Multiplex Fluorescent v2 kit (ACD #323100), and followed the manufacturer protocol (ACD #323100-USM) using probes for *Snap25* (ACD #516471), *Etv1* (ACD #557891-C3), and *Ntrk2* (ACD #423611-C2).

Images were acquired on a Keyence BZ-X710 microscope. MO infusion sites were consistent across mice and analyzed with the open access image analysis software, CellProfiler. Excitatory cell bodies were determined by *Snap25* expression, and within that population, layer IV and V cells were identified through *Etv1* expression (Boyle et al., 2011; Rowell et al., 2010). *Ntrk2* expression data were collected as puncta per *Etv1*+ or *Etv*1-neurons, and as percentage of *Etv1*+/− neurons that contained any *Ntrk2* puncta. *Ntrk2* was also quantified in *Snap25* + cells. Each mouse was considered an independent sample.

Dendritic spine imaging—Mice were euthanized 24 h after behavioral testing. Dendritic segments co-labeled with YFP (indicating excitatory deep-layer neurons) and RFP (indicating the tag on the control viral vector or the immunostained HA tag) were imaged with a spinning disk confocal microscope (VisiTech International) on a Leica microscope. Z-stacks were collected using a 0.1μm step size with a 100×1.4NA objective lens. Independent dendritic segments (4–8/mouse) were collected from each animal and imaged from secondary or tertiary basilar dendritic branches.

Semi-automated dendrite and dendritic spine reconstruction—Using the FilamentTracer module of Imaris (Bitplane AG), images were processed. Using the autodepth function, a dendritic segment 15–25μm in length was drawn. Dendrite diameter was determined via the FilamentTracer processing algorithms, since dendritic swelling

can be a sign of damage. Dendritic spines were reconstructed in 3D using the autodepth function and were classified using established parameters (Radley et al., 2013). Each mouse contributed a single density value (per animal average) for dendritic spine classification and dendrite length and width analyses. For spine length analyses, each spine contributed a single value. A single blinded rater processed all images within an experiment.

Spine clustering analyses were performed using "Spine Attachment Point Distance" values provided by Imaris reconstructions. Distances between one dendritic spine and its neighboring spine were determined by subtracting the listed value distances from each other (generating "interspine intervals", or ISIs). Group means were then calculated. Each ISI was converted to a z-score [z score = (ISI – group mean)/group standard deviation]. This approach allows us to analyze spine distance distribution while controlling for overall density.

QUANTIFICATION AND STATISTICAL ANALYSIS

Statistical analyses were performed using SPSS with α 0.05 throughout. n values are reported in the figure captions. Response rates, food intake, and binned *Ntrk2* puncta were compared by repeated measures ANOVA. In the case of significant interactions, Tukey's *post-hoc* tests were used, and results are indicated graphically. Value-based action refers to preferring the valued outcome at the probe test, reflected by significantly greater responding in the valued *vs.* devalued condition.

Ntrk2 puncta, dendritic spine densities, dendrite lengths, dendrite widths, and c-Fos + puncta were compared by *t*-tests. Dendritic spine lengths and distances were compared by Kolmogorov-Smirnov comparisons, with p   0.01 considered significant.

Throughout, values +/− 2 SDs from the mean were excluded from analyses, as in prior similar studies (Bradfield et al., 2015). Further, mice that did not exhibit a preference for the valued *vs.* devalued pellet during the post-probe consumption test or had misplaced infusions were excluded from analyses. These exclusions are summarized in Table S1. Group sizes were determined based on power analyses and similar prior experiments.

Sex differences—We never detected an effect of sex except for the CTA procedure in Figure 5D, in which case, consumption between males *vs.* females differed. A graph representing the sexes separately, along with the statistics, is provided in Figure S7. Importantly, sex differences in CTA seem unlikely to have affected the outcome of the experiment, as no effects of sex were detected by the conclusion of the CTA procedure or during the choice test, which determines whether mice modify their behavior based on the values of the pellets, or the post-probe consumption test.

Supplementary Material

Refer to Web version on PubMed Central for supplementary material.

ACKNOWLEDGMENTS

REFERENCES

Arana FS, Parkinson JA, Hinton E, Holland AJ, Owen AM, and Roberts AC (2003). Dissociable contributions of the human amygdala and orbitofrontal cortex to incentive motivation and goal selection. J. Neurosci 23, 9632–9638. 10.1523/jneurosci.23-29-09632.2003. [PubMed: 14573543]

Araya R, Vogels TP, and Yuste R. (2014). Activity-dependent dendritic spine neck changes are correlated with synaptic strength. Proc. Natl. Acad. Sci. USA 111, E2895–E2904. 10.1073/pnas.1321869111.

Balleine BW (2020). Corticostriatal intrusions. In Intrusive Thinking: From Molecules to Free Will, Kalivas PW and Paulus MP, eds. (The MIT Press), pp. 21–38.

Barfield ET, and Gourley SL (2017). Adolescent corticosterone and trkb pharmaco-manipulations sex-dependently impact instrumental reversal learning later in life. Front. Behav. Neurosci 11, 237. 10.3389/fnbeh.2017.00237. [PubMed: 29270114]

Barfield ET, and Gourley SL (2018). Prefrontal cortical trkB, glucocorticoids, and their interactions in stress and developmental contexts. Neurosci. Biobehav. Rev 95, 535–558. 10.1016/j.neubiorev.2018.10.015. [PubMed: 30477984]

Barfield ET, and Gourley SL (2019). Glucocorticoid-sensitive ventral hippocampal-orbitofrontal cortical connections support goal-directed action - curt Richter Award Paper 2019. Psychoneuroendocrinology 110, 104436. 10.1016/j.psyneuen.2019.104436.

Bechara A, Damasio AR, Damasio H, and Anderson SW (1994). Insensitivity to future consequences following damage to human prefrontal cortex. Cognition 50, 7–15. 10.1016/0010-0277(94)90018-3. [PubMed: 8039375]

Berry KP, and Nedivi E. (2017). Spine dynamics: are they all the same? Neuron 96, 43–55. 10.1016/j.neuron.2017.08.008. [PubMed: 28957675]

Boyle MP, Bernard A, Thompson CL, Ng L, Boe A, Mortrud M, Hawrylycz MJ, Jones AR, Hevner RF, and Lein ES (2011). Cell-type-specific consequences of reelin deficiency in the mouse neocortex, hippocampus, and amygdala. J. Comp. Neurol 519, 2061–2089. 10.1002/cne.22655. [PubMed: 21491433]

Bradfield LA, and Hart G. (2020). Rodent medial and lateral orbitofrontal cortices represent unique components of cognitive maps of task space. Neurosci. Biobehav. Rev 108, 287–294. 10.1016/j.neubiorev.2019.11.009. [PubMed: 31743727]

Bradfield LA, Dezfouli A, van Holstein M, Chieng B, and Balleine BW (2015). Medial orbitofrontal cortex mediates outcome retrieval in partially observable task situations. Neuron 88, 1268–1280. 10.1016/j.neuron.2015.10.044. [PubMed: 26627312]

Bradfield LA, Hart G, and Balleine BW (2018). Inferring action-dependent outcome representations depends on anterior but not posterior medial orbitofrontal cortex. Neurobiol. Learn. Mem 155, 463–473. 10.1016/j.nlm.2018.09.008. [PubMed: 30243849]

Bryant KG, and Barker JM (2020). Arbitration of approach-avoidance conflict by ventral hippocampus. Front. Neurosci 14, 615337. 10.3389/fnins.2020.615337. [PubMed: 33390895]

Burton AC, Kashtelyan V, Bryden DW, and Roesch MR (2014). Increased firing to cues that predict low-value reward in the medial orbitofrontal cortex. Cereb. Cortex 24, 3310–3321. 10.1093/cercor/bht189. [PubMed: 23901075]

Cahoy JD, Emery B, Kaushal A, Foo LC, Zamanian JL, Christopherson KS, Xing Y, Lubischer JL, Krieg PA, Krupenko SA, et al. (2008). A transcriptome database for astrocytes, neurons, and oligodendrocytes: a new resource for understanding brain development and function. J. Neurosci 28, 264–278. 10.1523/jneurosci.4178-07.2008. [PubMed: 18171944]

Cazorla M, Prémont J, Mann A, Girard N, Kellendonk C, and Rognan D. (2011). Identification of a low-molecular weight TrkB antagonist with anxiolytic and antidepressant activity in mice. J. Clin. Invest 121, 1846–1857. 10.1172/jci43992. [PubMed: 21505263]

Chakravarthy S, Saiepour MH, Bence M, Perry S, Hartman R, Couey JJ, Mansvelder HD, and Levelt CN (2006). Postsynaptic TrkB signaling has distinct roles in spine maintenance in adult visual cortex and hippocampus. Proc. Natl. Acad. Sci. USA 103, 1071–1076. 10.1073/pnas.0506305103. [PubMed: 16418274]

Chang S, Fang K, Zhang K, and Wang J. (2015). Network-based analysis of schizophrenia genome-wide association data to detect the joint functional association signals. PLoS One 10, e0133404. 10.1371/journal.pone.0133404. [PubMed: 26193471]

Dalton GL, Wang NY, Phillips AG, and Floresco SB (2016). Multifaceted contributions by different regions of the orbitofrontal and medial prefrontal cortex to probabilistic reversal learning. J. Neurosci 36, 1996–2006. 10.1523/jneurosci.3366-15.2016. [PubMed: 26865622]

DePoy LM, Shapiro LP, Kietzman HW, Roman KM, and Gourley SL (2019). β1-integrins in the developing orbitofrontal cortex are necessary for expectancy updating in mice. J. Neurosci 39, 6644–6655. 10.1523/jneurosci.3072-18.2019. [PubMed: 31253753]

dos Remedios CG, Chhabra D, Kekic M, Dedova IV, Tsubakihara M, Berry DA, and Nosworthy NJ (2003). Actin binding proteins: regulation of cytoskeletal microfilaments. Physiol. Rev 83, 433–473. 10.1152/physrev.00026.2002. [PubMed: 12663865]

Ehrengruber MU, Hennou S, Büeler H, Naim HY, Déglon N, and Lundstrom K. (2001). Gene transfer into neurons from hippocampal slices: comparison of recombinant Semliki Forest Virus, adenovirus, adeno-associated virus, lentivirus, and measles virus. Mol. Cell. Neurosci 17, 855–871. 10.1006/mcne.2001.0982. [PubMed: 11358483]

Eickholt BJ, Ahmed AI, Davies M, Papakonstanti EA, Pearce W, Starkey ML, Bilancio A, Need AC, Smith AJH, Hall SM, et al. (2007). Control of axonal growth and regeneration of sensory neurons by the p110δ PI 3-Kinase. PLoS One 2, e869. 10.1371/journal.pone.0000869. [PubMed: 17846664]

Fanselow MS, and Dong HW (2010). Are the dorsal and ventral hippocampus functionally distinct structures? Neuron 65, 7–19. 10.1016/j.neuron.2009.11.031. [PubMed: 20152109]

Feng G, Mellor RH, Bernstein M, Keller-Peck C, Nguyen QT, Wallace M, Nerbonne JM, Lichtman JW, and Sanes JR (2000). Imaging neuronal subsets in transgenic mice expressing multiple spectral variants of GFP. Neuron 28, 41–51. 10.1016/S0896-6273(00)00084-2. [PubMed: 11086982]

Ferreira G, Gutiérrez R, De La Cruz V, and Bermúdez-Rattoni F. (2002). Differential involvement of cortical muscarinic and NMDA receptors in short- and long-term taste aversion memory. Eur. J. Neurosci 16, 1139–1145. 10.1046/j.1460-9568.2002.02174.x. [PubMed: 12383243]

Galloway EM, Woo NH, and Lu B. (2008). Chapter 15 Persistent neural activity in the prefrontal cortex: a mechanism by which BDNF regulates working memory? In Progress in Brain Research, Sossin WS, Lacaille J-C, Castellucci VF, and Belleville S, eds. (Elsevier), pp. 251–266. 10.1016/S0079-6123(07)00015-5.

Gomez JL, Bonaventura J, Lesniak W, Mathews WB, Sysa-Shah P, Rodriguez LA, Ellis RJ, Richie CT, Harvey BK, Dannals RF, et al. (2017). Chemogenetics revealed: DREADD occupancy and activation via converted clozapine. Science 357, 503–507. 10.1126/science.aan2475. [PubMed: 28774929]

Gourley SL, Lee AS, Howell JL, Pittenger C, and Taylor JR (2010). Dissociable regulation of instrumental action within mouse prefrontal cortex. Eur. J. Neurosci 32, 1726–1734. 10.1111/j.1460-9568.2010.07438.x. [PubMed: 21044173]

Gourley SL, Zimmermann KS, Allen AG, and Taylor JR (2016). The Medial orbitofrontal cortex regulates sensitivity to outcome value. J. Neurosci 36, 4600–4613. 10.1523/jneurosci.4253-15.2016. [PubMed: 27098701]

Gutiérrez H, Hernández-Echeagaray E, Ramírez-Amaya V, and Bermúdez-Rattoni F. (1999). Blockade of N-methyl-d-aspartate receptors in the insular cortex disrupts taste aversion and spatial memory formation. Neuroscience 89, 751–758. 10.1016/S0306-4522(98)00360-1. [PubMed: 10199610]

Hartmann M, Brigadski T, Erdmann KS, Holtmann B, Sendtner M, Narz F, and Lessmann V. (2004). Truncated TrkB receptor-induced outgrowth of dendritic filopodia involves the p75 neurotrophin receptor. J. Cell Sci 117, 5803–5814. 10.1242/jcs.01511. [PubMed: 15507485]

Hartmann M, Heumann R, and Lessmann V. (2001). Synaptic secretion of BDNF after high-frequency stimulation of glutamatergic synapses. Embo j 20, 5887–5897. 10.1093/emboj/20.21.5887. [PubMed: 11689429]

Hayashi M, Mitsunaga F, Itoh M, Shimizu K, and Yamashita A. (2000). Development of full-length Trk B-immunoreactive structures in the prefrontal and visual cortices of the macaque monkey. Anat. Embryol 201, 139–147. 10.1007/PL00008234.

He XP, Kotloski R, Nef S, Luikart BW, Parada LF, and McNamara JO (2004). Conditional deletion of TrkB but not BDNF prevents epileptogenesis in the kindling model. Neuron 43, 31–42. 10.1016/j.neuron.2004.06.019. [PubMed: 15233915]

Hoover WB, and Vertes RP (2011). Projections of the medial orbital and ventral orbital cortex in the rat. J. Comp. Neurol 519, 3766–3801. 10.1002/cne.22733. [PubMed: 21800317]

Izquierdo A. (2017). Functional heterogeneity within rat orbitofrontal cortex in reward learning and decision making. J. Neurosci 37, 10529–10540. 10.1523/jneurosci.1678-17.2017. [PubMed: 29093055]

Jay TM, and Witter MP (1991). Distribution of hippocampal CA1 and subicular efferents in the prefrontal cortex of the rat studied by means of anterograde transport of Phaseolus vulgaris-leucoagglutinin. J. Comp. Neurol 313, 574–586. 10.1002/cne.903130404. [PubMed: 1783682]

Jenni NL, Li YT, and Floresco SB (2021). Medial orbitofrontal cortex dopamine D(1)/D(2) receptors differentially modulate distinct forms of probabilistic decision-making. Neuropsychopharmacology 46, 1240–1251. 10.1038/s41386-020-00931-1. [PubMed: 33452435]

Jenni NL, Rutledge G, and Floresco SB (2022). Distinct medial orbitofrontal–striatal circuits support dissociable component processes of risk/reward decision-making. J. Neurosci 42, 2743–2755. 10.1523/jneurosci.2097-21.2022. [PubMed: 35135853]

Kietzman HW, Shapiro LP, Trinoskey-Rice G, and Gourley SL (2022). Cell adhesion presence during adolescence controls the architecture of projection-defined prefrontal cortical neurons and reward-related action strategies later in life. Dev. Cogn. Neurosci 54, 101097. 10.1016/j.dcn.2022.101097. [PubMed: 35325840]

Kringelbach ML, and Rolls ET (2004). The functional neuroanatomy of the human orbitofrontal cortex: evidence from neuroimaging and neuropsychology. Prog. Neurobiol 72, 341–372. 10.1016/j.pneurobio.2004.03.006. [PubMed: 15157726]

Kusumoto-Yoshida I, Liu H, Chen BT, Fontanini A, and Bonci A. (2015). Central role for the insular cortex in mediating conditioned responses to anticipatory cues. Proc. Natl. Acad. Sci. USA 112, 1190–1195. 10.1073/pnas.1416573112. [PubMed: 25583486]

Laroche S, Davis S, and Jay TM (2000). Plasticity at hippocampal to prefrontal cortex synapses: dual roles in working memory and consolidation. Hippocampus 10, 438–446. 10.1002/1098-1063(2000)10:4<438:Aid-hipo10>3.0.Co;2-3. [PubMed: 10985283]

Li DC, Dighe NM, Barbee BB, Pitts EG, Kochoian B, Blumenthal SA, Figueroa J, Leong T, and Gourley SL (2022). A molecularly integrated amygdala-fronto-striatal network coordinates flexible learning and memory. Nat. Neurosci. In press.

Lichtenberg NT, Sepe-Forrest L, Pennington ZT, Lamparelli AC, Greenfield VY, and Wassum KM (2021). The medial orbitofrontal cortex–basolateral amygdala circuit regulates the influence of reward cues on adaptive behavior and choice. J. Neurosci 41, 7267–7277. 10.1523/jneurosci.0901-21.2021. [PubMed: 34272313]

Loh MK, Ferrara NC, Torres JM, and Rosenkranz JA (2022). Medial orbitofrontal cortex and nucleus accumbens mediation in risk assessment behaviors in adolescents and adults. Neuropsychopharmacology 47, 1808–1815. 10.1038/s41386-022-01273-w. [PubMed: 35039643]

Lustberg D, Iannitelli AF, Tillage RP, Pruitt M, Liles LC, and Weinshenker D. (2020). Central norepinephrine transmission is required for stress-induced repetitive behavior in two rodent

models of obsessive-compulsive disorder. Psychopharmacology (Berl) 237, 1973–1987. 10.1007/s00213-020-05512-0. [PubMed: 32313981]

Malvaez M, Shieh C, Murphy MD, Greenfield VY, and Wassum KM (2019). Distinct cortical-amygdala projections drive reward value encoding and retrieval. Nat. Neurosci 22, 762–769. 10.1038/s41593-019-0374-7. [PubMed: 30962632]

Manvich DF, Webster KA, Foster SL, Farrell MS, Ritchie JC, Porter JH, and Weinshenker D. (2018). The DREADD agonist clozapine N-oxide (CNO) is reverse-metabolized to clozapine and produces clozapine-like interoceptive stimulus effects in rats and mice. Sci. Rep 8, 3840. 10.1038/s41598-018-22116-z. [PubMed: 29497149]

Matsuda S, Ikeda Y, Murakami M, Nakagawa Y, Tsuji A, and Kitagishi Y. (2019). Roles of PI3K/AKT/GSK3 pathway involved in psychiatric illnesses. Diseases 7, E22. 10.3390/diseases7010022.

Michaelsen K, Zagrebelsky M, Berndt-Huch J, Polack M, Buschler A, Sendtner M, and Korte M. (2010). Neurotrophin receptors TrkB.T1 and p75NTR cooperate in modulating both functional and structural plasticity in mature hippocampal neurons. Eur. J. Neurosci 32, 1854–1865. 10.1111/j.1460-9568.2010.07460.x. [PubMed: 20955473]

Münster A, Sommer S, and Hauber W. (2020). Dopamine D1 receptors in the medial orbitofrontal cortex support effort-related responding in rats. Eur. Neuropsychopharmacol 32, 136–141. 10.1016/j.euroneuro.2020.01.008. [PubMed: 32029310]

Nakao T, Okada K, and Kanba S. (2014). Neurobiological model of obsessive–compulsive disorder: evidence from recent neuropsychological and neuroimaging findings. Psychiatry Clin. Neurosci 68, 587–605. 10.1111/pcn.12195. [PubMed: 24762196]

Nasser HM, Lafferty DS, Lesser EN, Bacharach SZ, and Calu DJ (2018). Disconnection of basolateral amygdala and insular cortex disrupts conditioned approach in Pavlovian lever autoshaping. Neurobiol. Learn. Mem 147, 35–45. 10.1016/j.nlm.2017.11.010. [PubMed: 29169849]

Papakonstanti EA, Ridley AJ, and Vanhaesebroeck B. (2007). The p110δ isoform of PI 3-kinase negatively controls RhoA and PTEN. EMBO J. 26, 3050–3061. 10.1038/sj.emboj.7601763. [PubMed: 17581634]

Parkes SL, Ferreira G, and Coutureau E. (2016). Acquisition of specific response–outcome associations requires NMDA receptor activation in the basolateral amygdala but not in the insular cortex. Neurobiol. Learn. Mem 128, 40–45. 10.1016/j.nlm.2015.12.005. [PubMed: 26740161]

Parkes SL, Ravassard PM, Cerpa J-C, Wolff M, Ferreira G, and Coutureau E. (2017). Insular and ventrolateral orbitofrontal cortices differentially contribute to goal-directed behavior in rodents. Cereb. Cortex 28, 2313–2325. 10.1093/cercor/bhx132.

Paulus MP, and Frank LR (2003). Ventromedial prefrontal cortex activation is critical for preference judgments. Neuroreport 14, 1311–1315. 10.1097/01.wnr.0000078543.07662.02. [PubMed: 12876463]

Pitts EG, Li DC, and Gourley SL (2018). Bidirectional coordination of actions and habits by TrkB in mice. Sci. Rep 8, 4495. 10.1038/s41598-018-22560-x. [PubMed: 29540698]

Plassmann H, O'Doherty J, and Rangel A. (2007). Orbitofrontal cortex encodes willingness to pay in everyday economic transactions. J. Neurosci 27, 9984–9988. 10.1523/jneurosci.2131-07.2007. [PubMed: 17855612]

Pontrello CG, and Ethell IM (2009). Accelerators, brakes, and gears of actin dynamics in dendritic spines. Open Neurosci. J 3, 67–86. 10.2174/1874082000903020067. [PubMed: 20463852]

Radley JJ, Anderson RM, Hamilton BA, Alcock JA, and Romig-Martin SA (2013). Chronic stress-induced alterations of dendritic spine subtypes predict functional decrements in an hypothalamo–pituitary–adrenal-inhibitory prefrontal circuit. J. Neurosci 33, 14379–14391. 10.1523/jneurosci.0287-13.2013. [PubMed: 24005291]

Raghavan S, Bauer C, Mundschau G, Li Q, and Fuchs E. (2000). Conditional ablation of beta1 integrin in skin. Severe defects in epidermal proliferation, basement membrane formation, and hair follicle invagination. J. Cell Biol 150, 1149–1160. 10.1083/jcb.150.5.1149. [PubMed: 10974002]

Rowell JJ, Mallik AK, Dugas-Ford J, and Ragsdale CW (2010). Molecular analysis of neocortical layer structure in the ferret. J. Comp. Neurol 518, 3272–3289. 10.1002/cne.22399. [PubMed: 20575059]

Rudebeck PH, and Izquierdo A. (2022). Foraging with the frontal cortex: a cross-species evaluation of reward-guided behavior. Neuropsychopharmacology 47, 134–146. 10.1038/s41386-021-01140-0. [PubMed: 34408279]

Rudebeck PH, and Rich EL (2018). Orbitofrontal cortex. Curr. Biol 28, R1083–R1088. 10.1016/j.cub.2018.07.018. [PubMed: 30253144]

Schilman EA, Uylings HBM, Galis-de Graaf Y, Joel D, and Groenewegen HJ (2008). The orbital cortex in rats topographically projects to central parts of the caudate-putamen complex. Neurosci. Lett 432, 40–45. 10.1016/j.neulet.2007.12.024. [PubMed: 18248891]

Schnider A, Nahum L, Pignat JM, Leemann B, Lövblad KO, Wissmeyer M, and Ptak R. (2013). Isolated prospective confabulation in Wernicke-Korsakoff syndrome: a case for reality filtering. Neurocase 19, 90–104. 10.1080/13554794.2011.654221. [PubMed: 22512690]

Schnider A, Treyer V, and Buck A. (2005). The human orbitofrontal cortex monitors outcomes even when no reward is at stake. Neuropsychologia 43, 316–323. 10.1016/j.neuropsychologia.2004.07.003. [PubMed: 15707609]

Sharp WG, Allen AG, Stubbs KH, Criado KK, Sanders R, McCracken CE, Parsons RG, Scahill L, and Gourley SL (2017). Successful pharmacotherapy for the treatment of severe feeding aversion with mechanistic insights from cross-species neuronal remodeling. Transl. Psychiatry 7, e1157. 10.1038/tp.2017.126. [PubMed: 28632204]

Stopper CM, Green EB, and Floresco SB (2012). Selective involvement by the medial orbitofrontal cortex in biasing risky, but not impulsive, choice. Cereb. Cortex 24, 154–162. 10.1093/cercor/bhs297. [PubMed: 23042736]

Verwer RW, Meijer RJ, Van Uum HF, and Witter MP (1997). Collateral projections from the rat hippocampal formation to the lateral and medial prefrontal cortex. Hippocampus 7, 397–402. 10.1002/(sici)1098-1063(1997)7:4<397::Aid-hipo5>3.0.Co;2-g. [PubMed: 9287079]

Wallis JD (2011). Cross-species studies of orbitofrontal cortex and value-based decision-making. Nat. Neurosci 15, 13–19. 10.1038/nn.2956. [PubMed: 22101646]

Wang CS, Kavalali ET, and Monteggia LM (2022). BDNF signaling in context: from synaptic regulation to psychiatric disorders. Cell 185, 62–76. 10.1016/j.cell.2021.12.003. [PubMed: 34963057]

Warren MS, Bradley WD, Gourley SL, Lin YC, Simpson MA, Reichardt LF, Greer CA, Taylor JR, and Koleske AJ (2012). Integrin β1 signals through Arg to regulate postnatal dendritic arborization, synapse density, and behavior. J. Neurosci 32, 2824–2834. 10.1523/jneurosci.3942-11.2012. [PubMed: 22357865]

Whyte AJ, Kietzman HW, Swanson AM, Butkovich LM, Barbee BR, Bassell GJ, Gross C, and Gourley SL (2019). Reward-related expectations trigger dendritic spine plasticity in the mouse ventrolateral orbitofrontal cortex. J. Neurosci 39, 4595–4605. 10.1523/jneurosci.2031-18.2019. [PubMed: 30940719]

Wikenheiser AM, Marrero-Garcia Y, and Schoenbaum G. (2017). Suppression of ventral hippocampal output impairs integrated orbitofrontal encoding of task structure. Neuron 95, 1197–1207.e3. 10.1016/j.neuron.2017.08.003. [PubMed: 28823726]

Witter MP (2006). Connections of the subiculum of the rat: topography in relation to columnar and laminar organization. Behav. Brain Res 174, 251–264. 10.1016/j.bbr.2006.06.022. [PubMed: 16876886]

Highlights

- TrkB in the MO supports selective outcome value memory updating to guide choice

- TrkB in the MO is not obviously necessary for value memory retrieval

- Hippocampal➔MO projections mediate outcome value updating under specific conditions

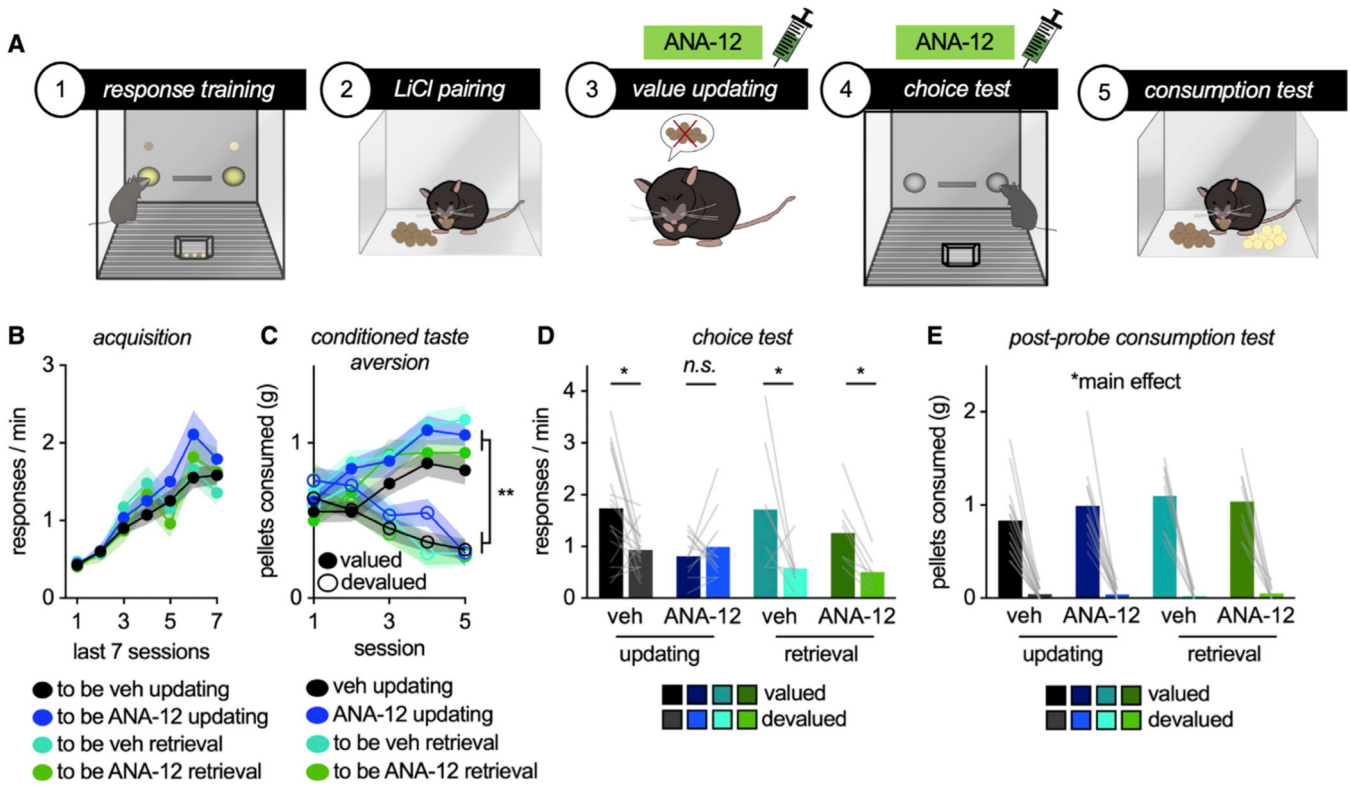- Hippocampal-MO coordination of value-based action is dependent on TrkB

Figure 1. TrkB is necessary for outcome-specific value memory updating, but not retrieval

(A) Schematic: Mice were trained to respond for 2 food pellets. Then, the value of 1 pellet was reduced via CTA. Whether mice updated their behavior was then measured in a choice test. Syringes indicate drug treatment during value updating or retrieval epochs.

(B) Response acquisition.

(C) Food consumption during CTA.

(D) TrkB inhibition during outcome value updating, but not retrieval, obstructed the ability of mice to preferentially respond for valued outcomes.

(E) Nevertheless, all groups preferentially consumed the valued versus devalued outcome during the post-probe consumption test. Symbols and shading, means ± SEMs; bars and lines connecting bars, means + individual data points; *p < 0.05, **p < 0.001. n.s., non-significant. n = 16 vehicle updating, n = 12 ANA-12 updating, n = 8 vehicle retrieval, n = 8 ANA-12 retrieval.
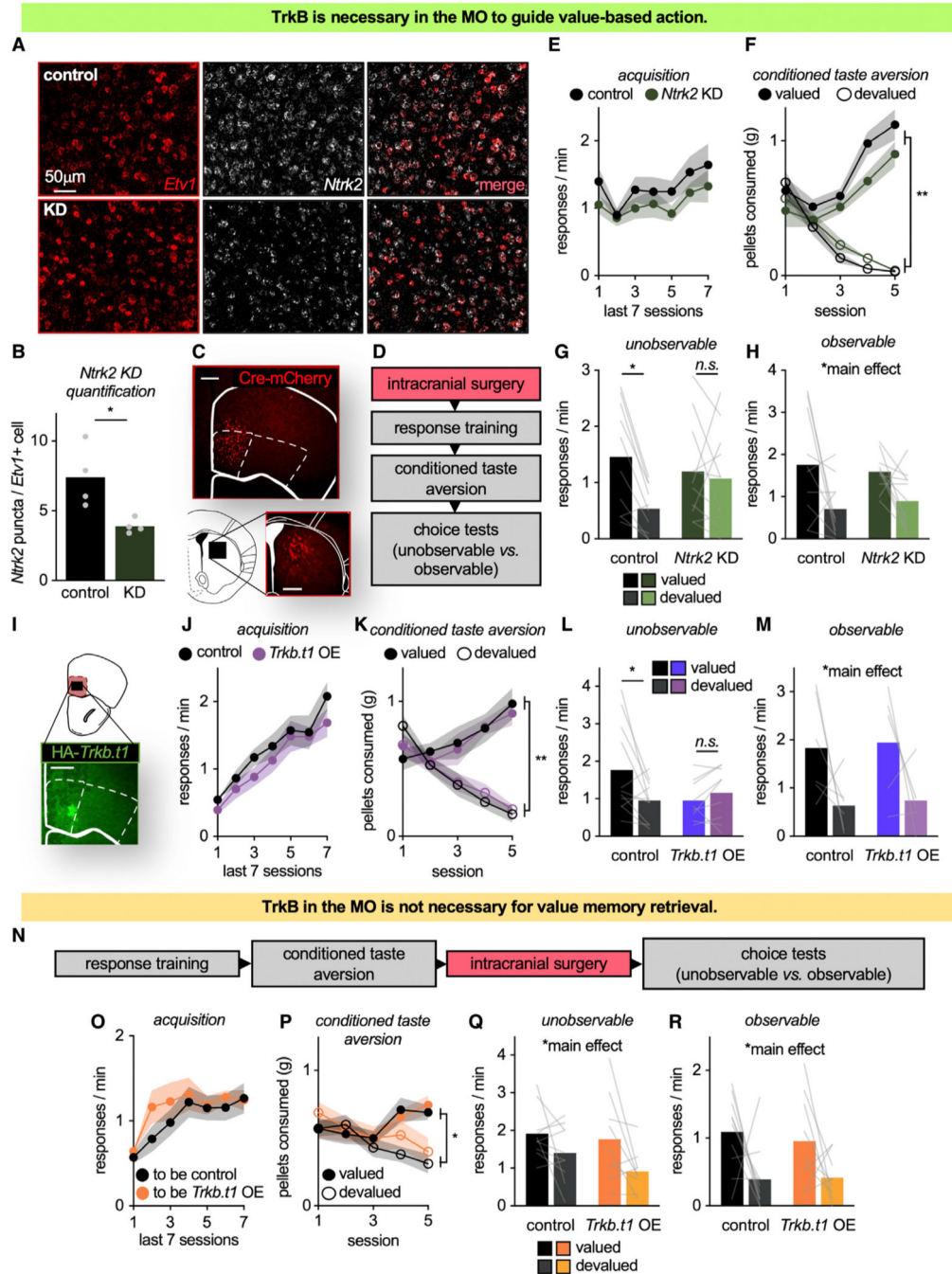
Figure 2. TrkB in the MO is necessary for outcome-specific value memory updating to guide future action selection

(A) *Ntrk2*-flox mice received mCherry ± Cre infusions into the MO to reduce *Ntrk2* in the Cre condition. Representative cells in the MO expressing *Etv1* and *Ntrk2* mRNA.

(B) *Ntrk2* puncta per *Etv1*+ cell was decreased in knockdown mice, confirming *Ntrk2* knockdown, including in layer V neurons.

(C) Representative infusion of Cre-mCherry into the MO, resulting in striatal innervation in a highly stereotyped fashion.

(D) Timeline.

(E) Response acquisition.

(F) Food consumption during CTA.

(G) During the unobservable choice test—meaning that outcomes were not delivered—MO *Ntrk2* knockdown mice failed to exhibit value-based action.

(H) When responses were reinforced, both groups preferentially responded for the valued outcome (n = 10 control, n = 11 *Ntrk2* KD).

(I) Representative infusion of HA-tagged *Trkb.t1* into the MO.

(J) Response acquisition.

(K) Food consumption during CTA.

(L) When outcomes were unobservable, *Trkb.t1* overexpression mice failed to exhibit value-based action (n = 11 control, n = 9 *Trkb.t1* OE).

(M) When responses were reinforced, both groups responded for the valued outcome (n = 6 control, n = 5 *Trkb.t1* OE).

(N) Timeline.

(O) Response acquisition.

(P) Food consumption during CTA.

(Q and R) When infusions followed the value updating period, *Trkb.t1* had no effects, with both groups favoring the valued outcome (n = 10 control, n = 9 *Trkb.t1* OE). Symbols and shading, means ± SEMs; bars and lines connecting bars, means + individual data points; *p < 0.05, **p < 0.001. KD, knockdown. OE, overexpression.
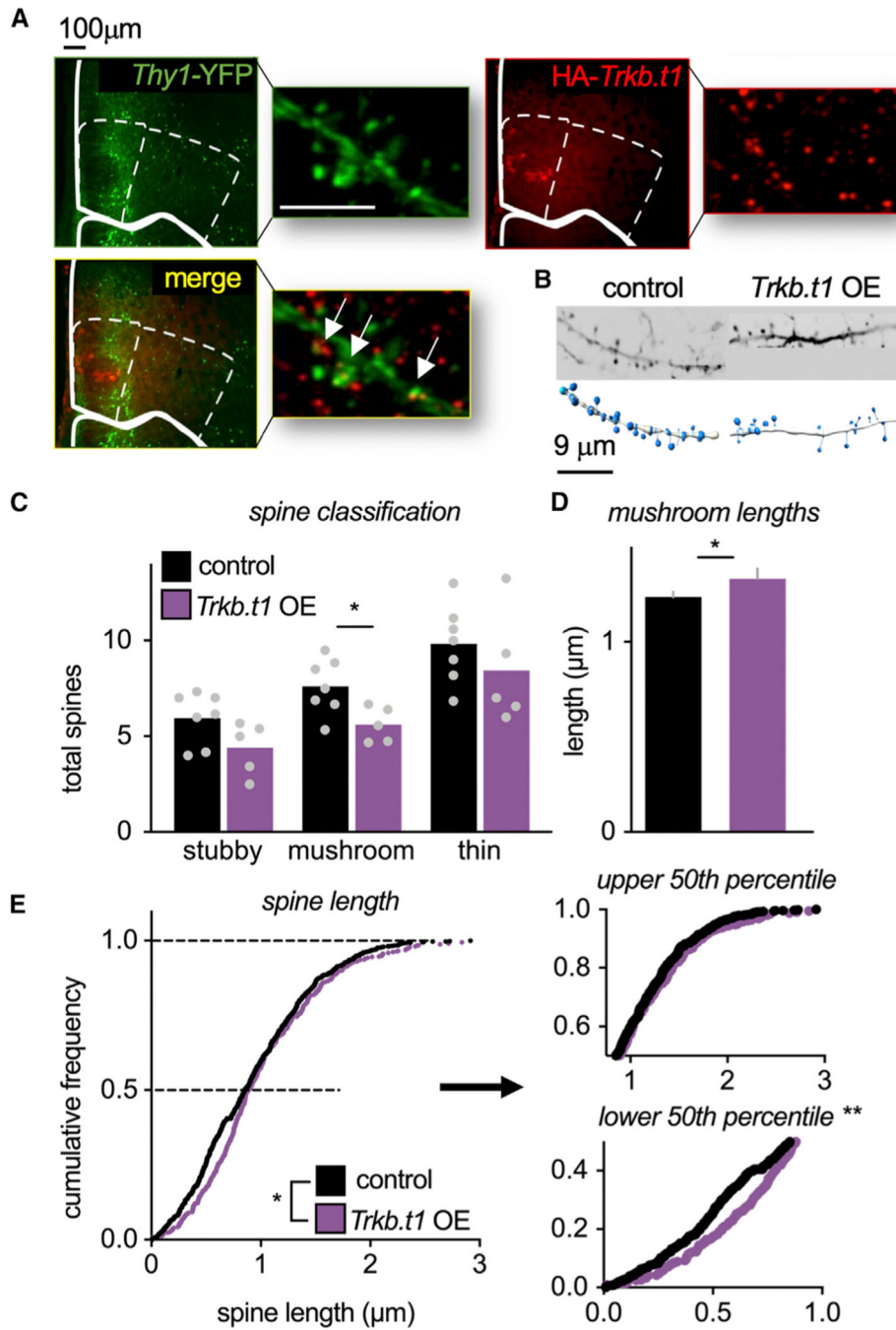
Figure 3. TrkB-mediated signaling controls dendritic spine structure on MO neurons

(A) Left: Representative images of yellow fluorescent protein (YFP)-expressing pyramidal neurons, red fluorescent protein (RFP)-tagged hemagglutinin (HA)-*Trkb.t1*, and co-labeled neurons. Scale bars, 5 μm.

(B) Representative dendrites.

(C) *Trkb.t1* overexpression reduced densities of mushroom-shaped spines (n = 7 control, n = 5 *Trkb.t1*).

(D) *Trkb.t1* overexpression lengthened mushroom-shaped spines in the MO (n = 302 control, n = 122 *Trkb.t1*).

(E) Overexpression of *Trkb.t1* lengthened spines, an effect localized to shorter spines (lower 50th percentile) (n = 976 control, n = 421 *Trkb.t1*).

(C) Bars and symbols, means + individual data points; (D) bars, means + SEMs (see Figure S3 for individual data points); (E) symbols, individual dendritic spines. *p < 0.05, **p < 0.001.
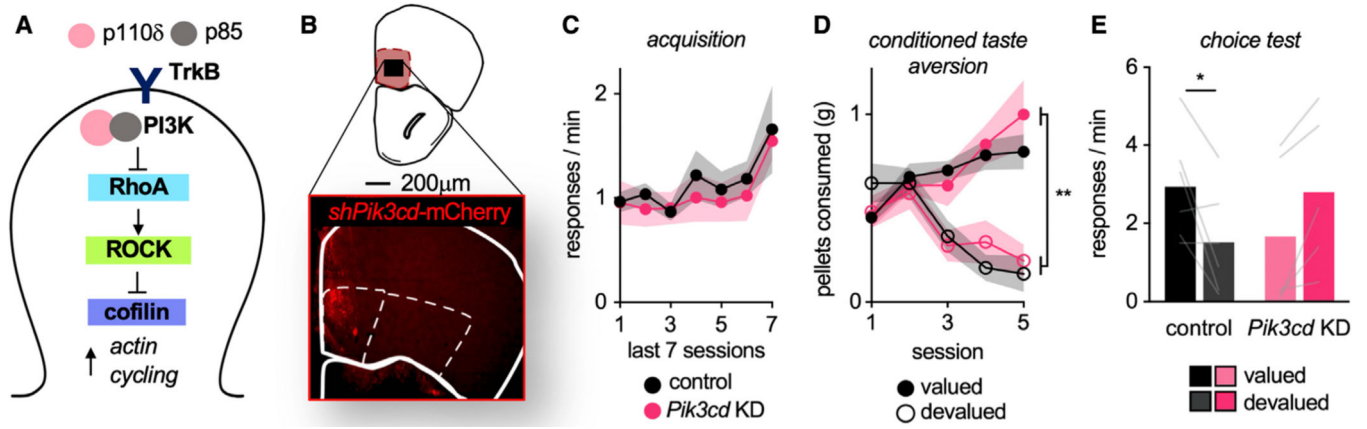
Figure 4. PI3K p110δ in the MO is necessary for value-based action

(A) Schematic of TrkB-PI3K signaling regulating spine structure through Rho kinase (ROCK) and cofilin.

(B) Representative infusion of mCherry-tagged sh-*Pik3cd* in the MO.

(C) Response acquisition.

(D) Food consumption during CTA.

(E) Reduction of p110δ in the MO impaired value-based action selection. Symbols and shading, means ± SEMs; bars and lines connecting bars, means + individual data points; *p < 0.05. n = 6 control and n = 5 *Pik3cd* KD.
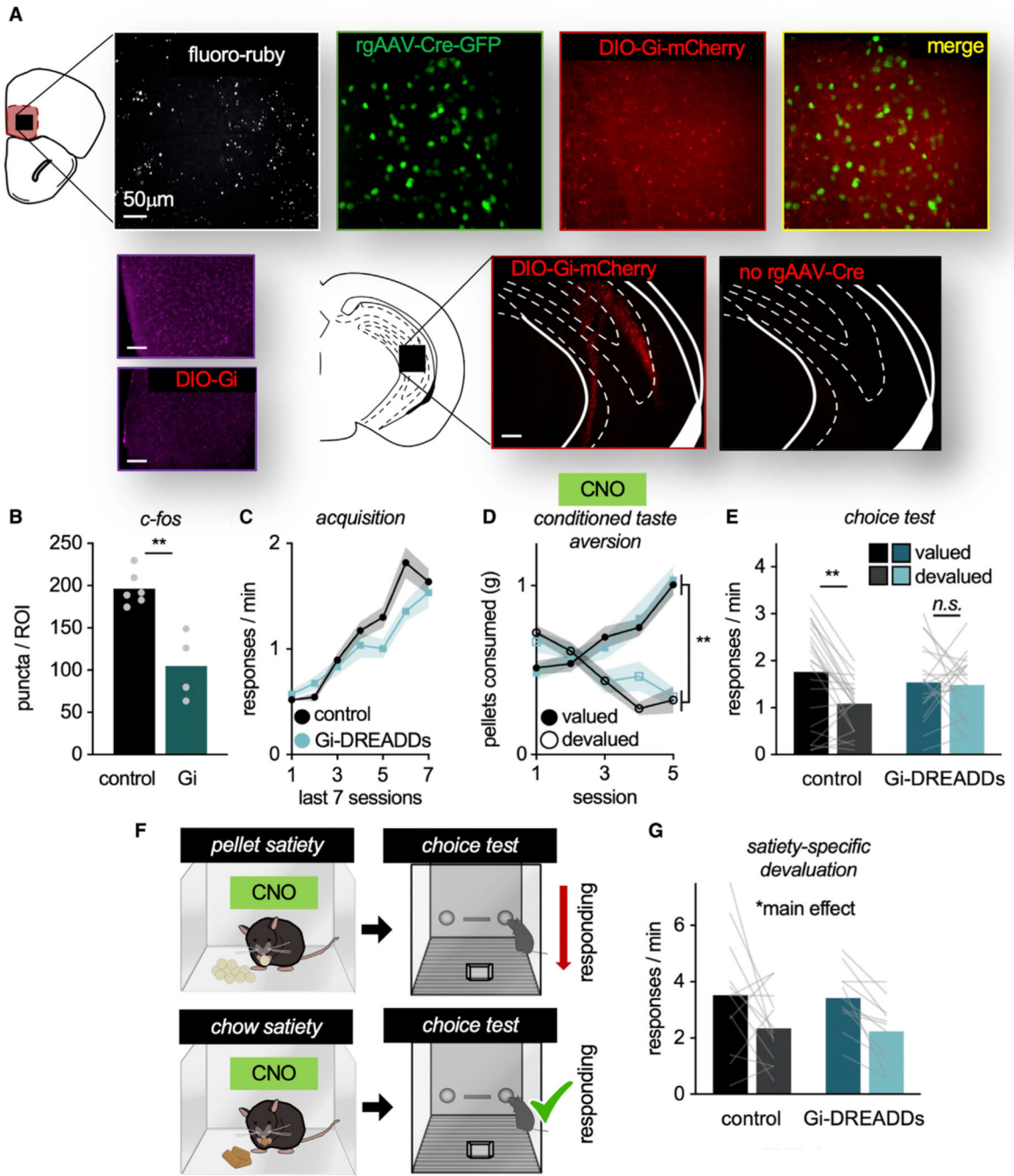
Figure 5. vHC-to-MO projections are necessary for mice to update outcome-specific value information upon CTA

(A) Representative images of: fluoro-ruby + terminals from the vHC in the MO, rgAAV-Cre-GFP in the MO co-labeled with DIO-Gi-DREADDs-mCherry from the vHC, and DIO-Gi-DREADDs-mCherry infusion in the vHC. Importantly, in the absence of rgAAV-Cre in the MO, DIO-Gi-DREADDs were not present in the vHC. Lower left: Representative images of c-Fos in the MO ± DIO-Gi-DREADDs.

(B) Following CNO, c-Fos was decreased in the DREADDs condition (n = 6 control, n = 4 Gi-DREADDs).

(C) Response acquisition. Response rates differed on sessions 5 (p = 0.037) and 6 (p = 0.025), likely a spurious effect of modest cohort differences. Groups did not differ on the final session.

(D) Food consumption during CTA.

(E) Inactivation of vHC-to-MO projections during the value-updating period obstructed later value-based choice (n = 24 control and n = 19 Gi-DREADDs).

(F) Schematic: Mice next received *ad libitum* access to one of the pellets before the choice test, devaluing that pellet. As a control, mice received *ad libitum* access to vivarium chow in a separate session. Mice received CNO before the prefeeding periods.

(G) Both groups inhibited responding for the devalued pellet, able to use value to guide actions following prefeeding (n = 13 control, n = 11 Gi-DREADDs). Symbols and shading, means ± SEMs; bars and lines connecting bars, means + individual data points; *p < 0.05, **p < 0.001.
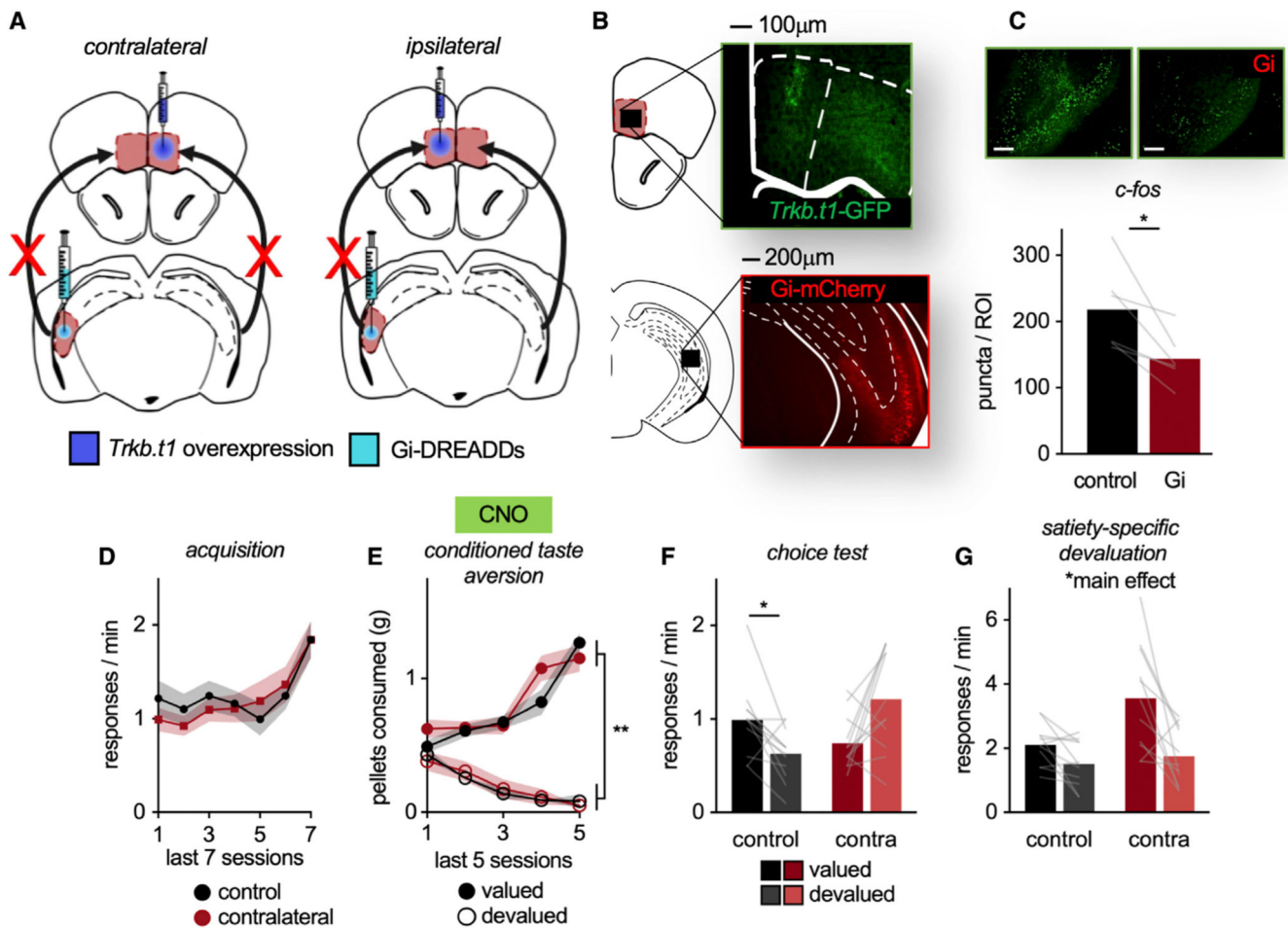
Figure 6. vHC-MO modulation of value-based action requires TrkB

(A) Schematic: Mice received *Trkb.t1* in one hemisphere of the MO and Gi-DREADDs in the contralateral vHC. With CNO, a healthy vHC projects to a TrkB activity-deficient MO and an inactivated vHC projects to a healthy MO, disrupting the circuit. Control mice receive unilateral infusions, leaving one hemisphere intact.

(B) Representative infusions of GFP-tagged *Trkb.t1* in the MO and Gi-DREADDs-mCherry in the vHC.

(C) Representative image of c-Fos in the vHC ± Gi-DREADDs. Following CNO, c-Fos was lower in hemispheres infused with Gi-DREADDs versus no DREADDs (n = 6).

(D) Response acquisition.

(E) Food consumption during CTA.

(F) Contralateral infusions impaired the ability of mice to use outcome-specific value information to influence action strategies, such that they failed to prefer the valued outcome.

(G) Mice also underwent a satiety-specific prefeeding devaluation test. In this case, both groups successfully inhibited responding to the devalued pellet. Symbols and shading, means ± SEMs; bars and lines connecting bars, means + individual data points; *p < 0.05, **p < 0.001. n = 12 control, n = 12 contralateral.
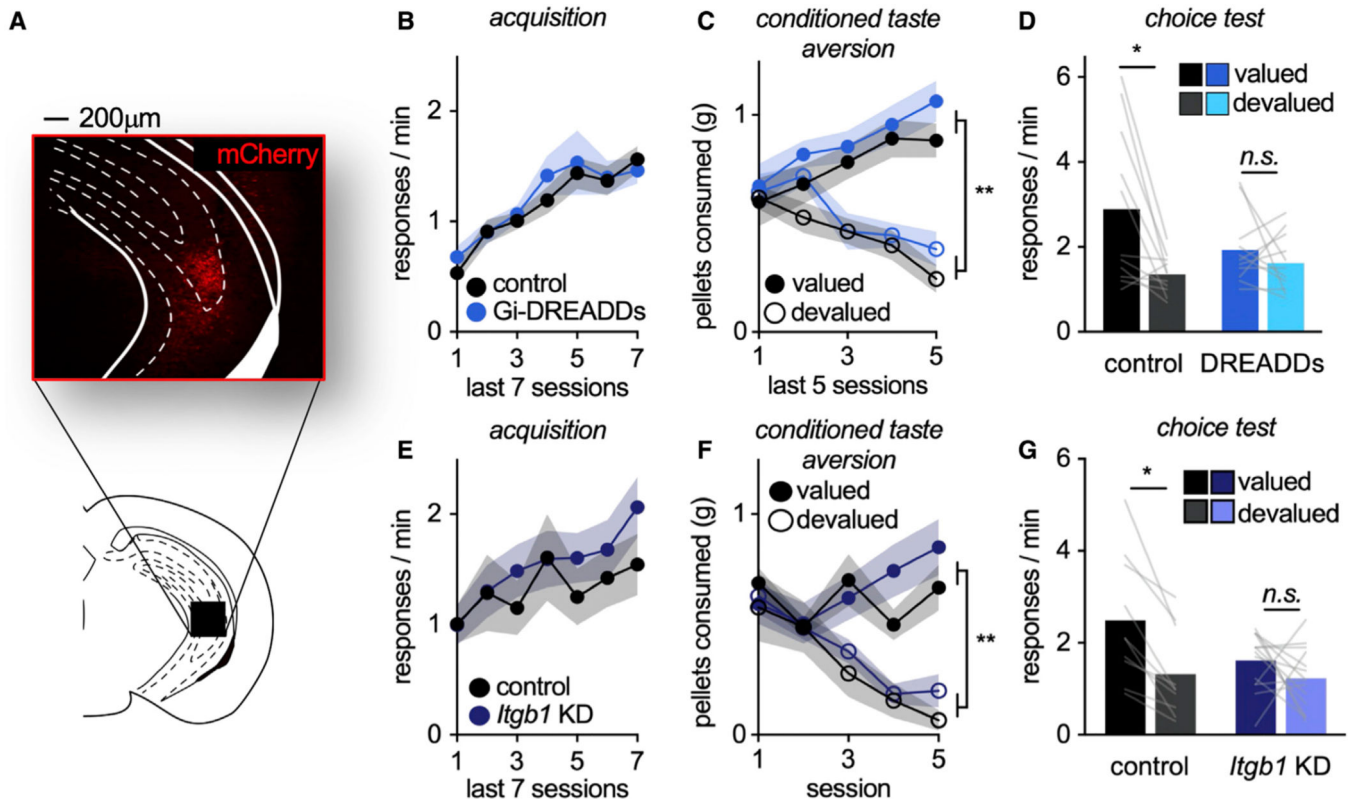
Figure 7. The vHC is necessary for value-based action following CTA

(A) Representative mCherry in the vHC.

(B) Response acquisition.

(C) Food consumption during CTA.

(D) Chemogenetic inhibition of the vHC during the value-updating period impaired value-based choice (n = 11 control, n = 11 DREADDs).

(E) In another experiment, we reduced *Itgb1* in the vHC. Response acquisition.

(F) Food consumption during CTA.

(G) *Itgb1* knockdown impaired the ability of mice to engage in value-based action, such that knockdown mice failed to prefer the valued outcome (n = 9 control, n = 14 *Itgb1* KD). Symbols and shading, means ± SEMs; bars and lines connecting bars, means + individual data points; *p < 0.05.

KEY RESOURCES TABLE

REAGENT or RESOURCE	SOURCE	IDENTIFIER
Antibodies		
Rabbit anti-c-Fos	Abcam	Cat.# ab190289 RRID: AB_2737414
Rabbit anti-HA	Millipore Sigma	Cat.# H6908; RRID: AB_260070
Goat anti-Rabbit, Alexa Fluor 488	Jackson ImmunoResearch	Cat.# 111-545-144; RRID: AB_2338052
Goat anti-Rabbit, Alexa Fluor 647	Jackson ImmunoResearch	Cat.# 111-605-144; RRID: AB_2338078
Goat anti-Rabbit, Peroxidase	Vector Laboratories	Cat.# PI-1000; RRID: AB_2336198
Streptavidin Cy5	Vector Laboratories	Cat.# SA-1500-1
Streptavidin Dylight 594	Vector Laboratories	Cat.# SA-5594-1
Bacterial and Virus Strains		
AAVrg-hSyn-HI-eGFP-Cre-WPRE-SV40	James M. Wilson	Addgene #105540-AAVrg
AAV5-hSyn-DIO-hM4D(Gi)-mCherry	Bryan Roth	Addgene #44362-AAV5
AAVrg-hSyn-DIO-mCherry	Bryan Roth	Addgene #50459-AAVrg
AAV5-CaMKII-hM4D(Gi)-mCherry	Bryan Roth	Addgene #50477-AAV5
AAV2-CaMKII-mCherry-Cre	UNC Viral Vector Core	N/A
AAV5-CaMKII-mCherry-Cre	UNC Viral Vector Core	N/A
AAV2-CaMKII-m*Pik3cd*-shRNA-mCherry	Vector Biolabs	Cat.# shAAV-250812
Fluoro-ruby	Millipore Sigma	Cat.# AG335
LV-CMV-*Trkb.t1*	Emory Viral Vector Core	N/A
LV-CMV-GFP	Emory Viral Vector Core	N/A
LV-CMV-RFP	Emory Viral Vector Core	N/A
Chemicals, Peptides, and Recombinant Proteins		
ANA-12	Millipore Sigma	Cat.# 219766-25-3
Clozapine-N-oxide	RTI International	Cat.# C-929
Lithium Chloride	Millipore Sigma	Cat.# 203637
Experimental Models: Organisms/strains		
Mouse: C57BL/6	The Jackson Laboratory	Stock #000664
Mouse: *Itgb1*^{tm1Efu}/J	The Jackson Laboratory	Stock #004605
Mouse: *Ntrk2*$^{flox/flox}$	He et al., 2004	N/A
Mouse: Thy1-YFP-H	The Jackson Laboratory	Stock #003782
Software and Algorithms		
CellProfiler	Beth Cimini	http://www.cellprofiler.org
Imaris v.8	Oxford Instruments	http://imaris.oxinst.com
ImageJ	Wayne Rasband	http://imagej.nih.gov/ij/
SPSS v.28	IBM	http://www.ibm.com/products/spss-statistics
Prism v.9	GraphPad	http://www.graphpad.com/scientific-software/prism

REAGENT or RESOURCE	SOURCE	IDENTIFIER
Other		
RNAScope Multiplex Fluorescent v2 Kit	ACD Bio	Cat.# 323100-USM
Etv1	ACD Bio	Cat.# 557891-C3
Ntrk2	ACD Bio	Cat.# 423611-C2
Snap25	ACD Bio	Cat.# 516471